

Effects of climate change on inter-basin exchange in Lower Lake Constance

Irene Caramatti¹, Frank Peeters¹, and Hilmar Hofmann¹

¹University of Konstanz

November 23, 2022

Abstract

Inter-basin exchange of water and dissolved substances in lakes is often limited by topographic constrictions leading to spatially heterogeneous distributions of nutrients and plankton. Here, we identify the main factors controlling inter-basin exchange on seasonal and inter-annual time scales and investigate the impact of changes in climate and hydrology focusing mainly on the exchange between two basins of Lower Lake Constance (LLC). The analysis is based on multi-annual simulations of LLC, a sensitivity analysis, and numerical tracer experiments with a coupled 3-D hydrodynamic ice model (AEM3D). The seasonal course of water exchange is predominantly determined by the seasonal change in the current speed across the sill, v_S , but also by changes in the area of the cross-section above the sill resulting from water level changes. The seasonal pattern of v_S is linked to the presence of ice cover, the seasonal change in stratification and in water level. The impact of climate warming and hydrological change on water exchange therefore varies seasonally. Climate warming results in reduced ice cover and an earlier onset and longer duration of stratification, leading to enhanced inter-basin exchange especially during winter and spring, but not in summer. In contrast, increased water levels enhance inter-basin exchange especially in summer, because the increase in cross-sectional area associated with increased water levels coincides then with high v_S . Finally, the fraction of water from Upper Lake Constance reaching the rather secluded basin Gnadensee increases with climate warming, implying a larger influence of the upstream conditions on Gnadensee.

Effects of climate change on inter-basin exchange in Lower Lake Constance

I. Caramatti¹, H. Hofmann¹ and F. Peeteers¹

¹ University of Konstanz, Konstanz, Germany

Corresponding author: Irene Caramatti (irene.caramatti@uni-konstanz.de)

Key Points:

- Inter-basin water exchange in Lower Lake Constance is characterized by a seasonal pattern
- The seasonal course of inter-basin exchange is predominantly determined by the seasonal change of exchange velocity
- The impact of climate warming and hydrological changes on inter-basin exchange varies seasonally

Abstract

Inter-basin exchange of water and dissolved substances in lakes is often limited by topographic constrictions leading to spatially heterogeneous distributions of nutrients and plankton. Here, we identify the main factors controlling inter-basin exchange on seasonal and inter-annual time scales and investigate the impact of changes in climate and hydrology focusing mainly on the exchange between two basins of Lower Lake Constance (LLC). The analysis is based on multi-annual simulations of LLC, a sensitivity analysis, and numerical tracer experiments with a coupled 3-D hydrodynamic ice model (AEM3D). The seasonal course of water exchange is predominantly determined by the seasonal change in the current speed across the sill, v_s , but also by changes in the area of the cross-section above the sill resulting from water level changes. The seasonal pattern of v_s is linked to the presence of ice cover, the seasonal change in stratification and in water level. The impact of climate warming and hydrological change on water exchange therefore varies seasonally. Climate warming results in reduced ice cover and an earlier onset and longer duration of stratification, leading to enhanced inter-basin exchange especially during winter and spring, but not in summer. In contrast, increased water levels enhance inter-basin exchange especially in summer, because the increase in cross-sectional area associated with increased water levels coincides then with high v_s . Finally, the fraction of water from Upper Lake Constance reaching the rather secluded basin Gnadensee increases with climate warming, implying a larger influence of the upstream conditions on Gnadensee.

Plain Language Summary

Heterogeneous conditions within a lake can be caused by topographic constrictions, e.g. a shallow sill, that limit inter-basin exchange of water and nutrients. Here, we identify the factors controlling inter-basin exchange between two sill-separated basins of Lower Lake Constance (LLC) and its modification due to climate warming and water level changes. The analysis was conducted with a three-dimensional model to simulate hydrodynamic conditions and ice cover formation in the lake and their modifications due to warmer air temperature and increased/decreased water level. Results showed that inter-basin exchange in the lake is high in summer and low in winter, especially in ice-covered months. The seasonal changes are mainly determined by changes in current speed across the sill and in the area of the cross-section above the sill resulting from water level changes. The impact of climate warming and hydrological change on water exchange varies seasonally: climate warming results in reduced ice cover and earlier stratification, enhancing inter-basin exchange in winter and spring, whereas increased water level enhances it especially in summer.

1 Introduction

Hydrodynamic processes affect bio-geochemistry, water exchange and the distribution of dissolved substances and suspended particles in lakes (Rueda & Cowen, 2005). Topographic constrictions, such as a shallow sill separating semi-enclosed basins from the main basin of a lake, can substantially limit inter-basin exchange and thus cause spatially heterogeneous distributions of nutrients, other water constituents, and plankton. Identification of the main factors controlling the exchange between semi-enclosed basins and the main water body is important for the assessment of potential consequences of climate change and associated changes in hydrology for inter-basin exchange and for the resulting distributions of dissolved substances and organisms.

Transport in lakes is predominantly controlled by wind forcing, ice cover suppressing wind forcing at the lake surface, stratification, river inflow, and water level determining the effective cross sections for inter-basin exchange across sills. All these factors are affected by climate change and hydrologic alterations in the catchments of lakes. E.g. climate warming reduces ice cover formation and duration (Magnuson et al., 2000), causes earlier ice breakup and thus longer periods of water column stratification, and results in warmer surface water temperature, increased stratification, and heat storage during summer (Livingstone 2003; Mishra et al., 2011; O'Reilly et al., 2015). Reduced or absent ice cover leads to more energetic winter circulation driven by wind shear on the open water (Fujisaki et al., 2013), whereas stronger stratification during summer may restrict the transfer of wind forcing input to horizontal currents in a narrower surface layer and may thus result in larger wind-driven surface currents (Bennett, 1974). Climate change and/or modifications of the hydrology in the catchment of lakes may

modify the water level dynamics in lakes (Haghighi & Kløve, 2015) thus also affect inter-basin exchange across sills.

Exchange of water and dissolved substances has been studied in lakes using different approaches ranging from tracer measurements to numerical models. E.g., field data on tracers and inverse modelling of tracer concentrations combining a simple inter-basin exchange model with vertical transport have been employed to investigate deep water renewal in Lake Baikal (Weiss, Carmack, & Koropalov, 1991; Hohmann et al., 1998; Peeters, 2000). Similar tracer studies and exchange models have been used to demonstrate that horizontal exchange between sill-separated lake basins during winter can be a dominant process controlling deep water renewal and deep water oxygenation in lakes (Aeschbach-Hertig et al., 1996; Schlatter et al., 1997). In these studies, as well as in MacIntyre et al. (2002), inter-basin exchange is mainly driven by inter-basin density differences. Other mechanisms affecting inter-basin exchange were discussed by Bartish (1987), e.g. riverine inflow, pressure-gradient-driven subsurface flows as cumulative result of wind-driven surface flows, flushing due to oscillating seiche motions, and turbulent horizontal diffusion.

During the last decades, three-dimensional (3-D) hydrodynamic models have been increasingly used to investigate hydrodynamics in lakes (e.g. Hodges et al., 2000; Beletsky & Schwab, 2001; Appt et al., 2004; Razmi et al., 2014; Wahl & Peeters, 2014; Dissanayake et al., 2019), but numerical simulations focusing on the exchange between sub-basins in lakes are not very common. One of the first applications of a 3-D hydrodynamic model to study the inter-basin exchange in standing freshwaters was focused on the exchange between a freshwater embayment and Lake Ontario through a long, shallow channel (Rueda & Cowen, 2005). Rao et al. (2009) simulated the circulation and the temperature and pollutant distribution in Hamilton Bay in Lake

Ontario, and the exchange between a harbor and the lake. In Lake Huron, a 3-D hydrodynamic model was combined with field measurements and drifter experiments to examine exchange between the open lake and the Saginaw Bay during summer months of three consecutive years (Nguyen et al., 2014). The exchange in the same system was also studied during the winter season by employing the same model coupled with an ice model (Nguyen et al., 2017). This study demonstrated that the ice cover significantly dampens water movement producing almost stagnant conditions around February in the Saginaw Bay (Nguyen et al., 2017). This result agreed with the study of Fujisaki et al. (2013) showing that ice cover slowed down surface water velocities in Lake Erie.

Three-dimensional hydrodynamic models have also been employed to assess the implication of modified boundary conditions on hydrodynamics and inter-basin exchange. Niu et al. (2015) investigated the sensitivity of inter-basin exchange in the three basins of Lake Erie to modification of the thermal regime. The effect of modifications of the wind field on inter-basin exchange has also been investigated, e.g., in Lake Taihu (China) (Liu et al., 2018), in Lake Geneva (Switzerland) (Umlauf & Lemmin, 2005), and in Lake Argyle (Western Australia) (Woodward et al., 2017).

However, most of these studies were conducted in very large lakes and focused on short, selected time periods. In the study here, we employed a 3-D model to investigate the exchange between sill-separated basins in detail resolving seasonal time scales in multi-annual simulations. With this approach, we assess to which extent climate warming and water level changes affect inter-basin exchange at seasonal time scales. The 3-D Aquatic Ecosystem Model (AEM3D) was used to simulate hydrodynamic conditions in Upper (ULC) and Lower Lake Constance (LLC), investigating in detail the water exchange between the basins of LLC in nine consecutive years.

The main focus was on the water exchange between Gnadensee (GS) and the adjacent basin Zeller See (ZS), which are separated by a shallow sill. The model was employed to study the main drivers of water exchange and its modifications due to climate warming and hydrological changes. Additionally, we conducted numerical tracer experiments providing information on the spreading of the water from the main tributary to LLC, river Seerhein, which originates from ULC and enters into the basin Rheinsee, from where its water spreads via ZS into GS. We hypothesized that climate warming and water level changes alter the water exchange between GS and ZS and the contribution of water from Seerhein in GS not only in absolute terms but also the seasonal patterns of the exchange.

In the following, we first explain the lake system, provide details on the model and the numerical simulations, and describe the scenarios considered. Afterwards we present and discuss the results from our numerical investigations.

2 Methods

2.1 Study site

Lake Constance (LC, Germany) is a large pre-alpine lake of glacial origin (Fig. 1). The lake consists of two main parts, Upper Lake Constance (ULC) and downstream Lower Lake Constance (LLC), which is connected to ULC via river Seerhein (Fig. 1c). ULC has a surface area of 473 km² and a maximum depth of about 251 m, whereas LLC has a surface area of 63 km² and maximum and mean depth of 46 m and 25 m, respectively.

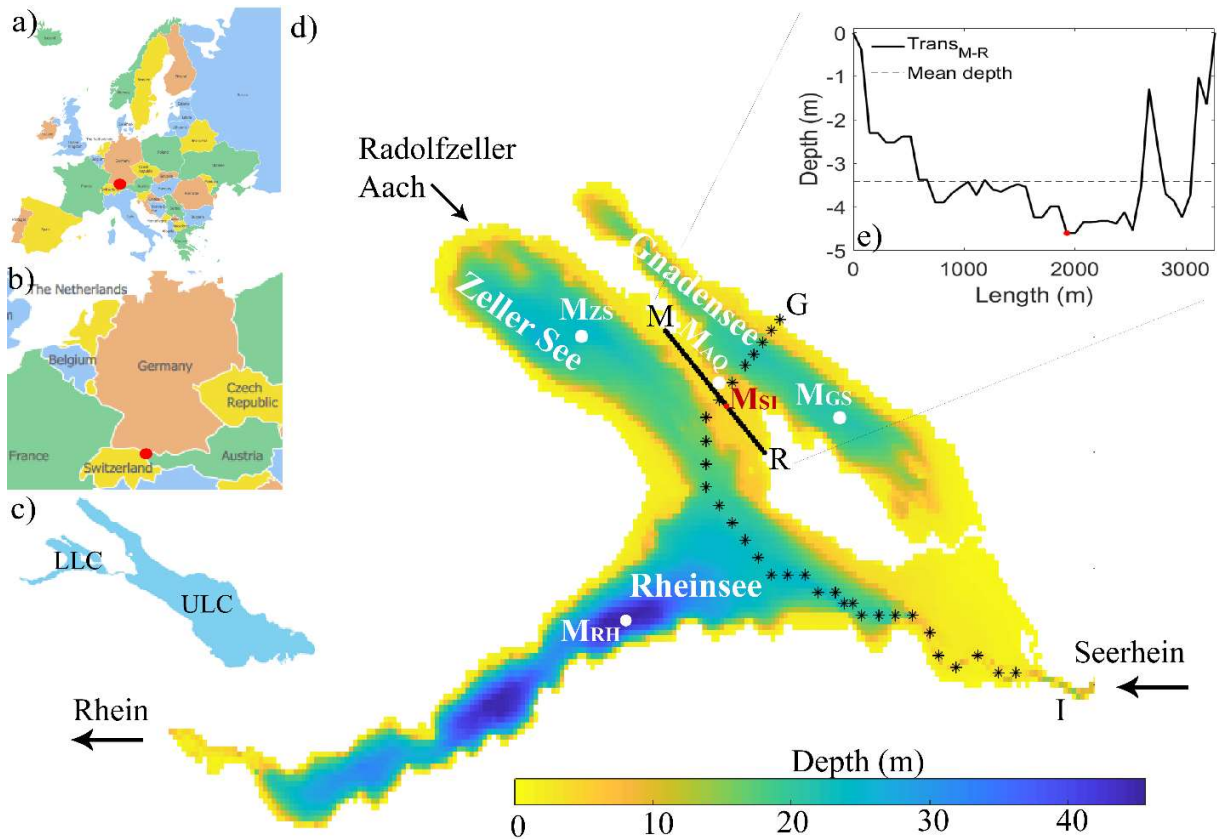


Figure 1: Schematic sketch of the study site. a) and b) Location of Lake Constance in Europe. c) Lake Constance subdivided in Upper Lake Constance (ULC) and Lower Lake Constance (LLC). d) Bathymetry of Lower Lake Constance indicating the sub-basins Gnadensee, Zeller See and Rheinsee and the main inflows (Seerhein and Radolfzeller Aach) and the outflow (Rhein). The transect $Trans_{M-R}$ along the sill between Gnadensee and Zeller See is represented by a black line, while $Trans_{I-G}$ by black asterisks. Monitoring stations M_{GS} (Gnadensee), M_{ZS} (Zeller See), M_{RH} (Rheinsee), M_{AQ} (HR Current Profiler, Current Profiler, Aquadopp) are indicated by white circles, while M_{SI} , the deepest station along $Trans_{M-R}$, by a red one. e) Depth contour (solid line), mean water depth (dashed line) and M_{SI} (red point) of $Trans_{M-R}$. The depth is measured relative to a water level of 395 m.a.s.l..

LLC is subdivided into three sub-basins (Fig. 1d) that differ in maximum water depth, hydro-geological features, thermal structure, ice formation and coverage (Caramatti et al., 2020), phytoplankton community and nutrient distributions (IGKB 2018). Rheinsee (RS) is the most southern basin with a maximum water depth of 46 m. In the north, RS is connected to Zeller See (ZS), which has a maximum water depth of 24 m. The most northern sub-basin of LLC is Gnadensee (GS) with a maximum water depth of 20 m. GS is the most enclosed sub-basin. It has no significant inflows and is connected to ZS only via a shallow sill of about 3.3 km length. The sill extends from the peninsula of Mettnau to the island of Reichenau (Fig. 1d,e) and has a mean and maximum depth of 3.4 m and 4.6 m, respectively, relative to a water level of 395 m.a.s.l. River Seerhein, which is the discharge from ULC and the main inflow into LLC, enters in the most eastern part of RS. The second largest inflow to LLC is the river Radolfzeller Aach, which enters in the most western part of ZS. The outflow of LLC is located in the most western part of RS (Fig.1d).

A specific emphasis of this investigation is on the water exchange across the sill between GS and ZS. Model results are therefore evaluated at 42 regular spaced stations between M and R on a transect along the sill, denoted as $\text{Trans}_{\text{M-R}}$ (Fig. 1d,e). $\text{Trans}_{\text{M-R}}$ follows a straight line that is turned clockwise at angle 47.6° to the west-east axis. The deepest station on the sill is M_{SI} . In addition, we investigate the transport of dissolved and suspended substances from the inflow Seerhein to GS and consider 32 stations along a 12 km long transect between I and G, $\text{Trans}_{\text{I-G}}$ (Fig. 1d).

Lower Lake Constance is typically stratified from April to November and inversely-stratified during winter months (January-March), when LLC develops regularly partial or complete ice cover (Caramatti et al., 2020). Further, the lake can be considered as dimictic

showing complete mixing during autumn overturn as well as after ice-off. During the last decade only in the years 2010, 2011, 2012 and 2017 ice cover developed in all three sub-basins of LLC, whereas full areal ice cover developed frequently in GS.

The water level of Lake Constance is unregulated and is mainly determined by the Alpine climate determining the discharge of river Rhein, the main tributary to ULC. The water level in ULC and LLC shows a pronounced seasonal course, with highest levels in summer due to inflow of melt water from the Alps and lowest levels at the end of February, when precipitation is stored as snow in the mountains of the catchment (Fig. 2b). The seasonal amplitude of the water level in LLC in the years 1991 – 2019 ranged between 1.0 and 2.9 m.

2.2 Model description

We used the 3-D Hydrodynamic-Aquatic Ecosystem Model (AEM3D, Hodges & Dallimore, 2018) to study the inter-annual and seasonal water exchange between GS and ZS in LLC under different forcing scenarios. The model was applied by coupling a coarse model for LC with a refined model for LLC. This model set up was already successfully employed to simulate the thermal structure and ice cover formation in LLC for 9 consecutive years (Caramatti et al., 2020).

The hydrodynamic model, which is based on ELCOM, solves the three-dimensional unsteady Reynolds-averaged Navier-Stokes equations, and scalar transport equations to model velocity and temperature distributions in space and time (Hodges, 2000). The equations are solved numerically using a Cartesian Arakawa C-grid in the horizontal dimension and the vertical discretization is based on fixed Z-layers (Hodges, 2000). Scalars and momentum are mixed vertically according to the amount of turbulent kinetic energy available from wind stirring

and shear production compared to the potential energy due to the water column stratification (Laval et al., 2003). The model includes Earth rotation, wind stress at the surface, surface thermal forcing, inflows and outflows. The hydrodynamic model is coupled to an ice module (Hodges & Dallimore, 2018). More details can be found in Hodges (1998), Oveisy et al. (2012) and Hodges and Dallimore (2018).

2.3 Model set up and validation

LLC was represented by a regular horizontal computational grid of 100 x 100 m and 79 vertical layers, whose thickness varies with depth. The vertical resolution was 0.5 m in the upper 60 layers and 1 m in the lowest 15 layers. Between the 61th and the 64th layer the vertical resolution increased gradually from 0.5 to 1 m. Time series of discharge and water temperature were prescribed at the locations of the inflows Seerhein and Radolfzeller Aach. The time series of the discharge at the outflow from LLC (river Rhein) was derived from a water balance based on the measured inflows and the measured change in water level (gauge Berlingen). The time series of the water temperature of river Seerhein was derived from the simulation of LC. LC was represented by a horizontal computational grid of 300 x 300 m and 70 vertical layers (Text S1). The data for all other inflows (temperatures and discharges) were provided by the Landesanstalt fuer Umwelt Baden-Wuerttemberg (LUBW), the Federal Office for the Environment of Switzerland (BAFU) and the Hydrographic Service Vorarlberg (VA).

Water temperature in LLC was initialized using temperature profiles measured with a CTD-probe (RBR) at the stations M_{ZS}, M_{GS} and M_{RH} that were interpolated internally by the model using an inverse distance weighting method. A spatially resolved wind field was obtained by linear interpolation of the horizontally resolved COSMO wind field of MeteoSwiss

(resolution of 2.2 km before April 2016 and 1.1 km afterwards, Doms et al., 2018) to the computational grid. Except for the wind field, the model was driven with horizontally uniform meteorological data (German Weather Service - DWD, station Konstanz). The model was operated by conducting continuous simulations from 4 March 2009 to 31 March 2018. For more details on model set up and input data see Caramatti et al. (2020).

The accuracy of the model to simulate the lake thermal structure and ice cover formation over the simulated period was evaluated in Caramatti et al. (2020). In the study here, we additionally compared simulated currents with currents measured with the Aquadopp Profiler HR (Nortek) at location M_{AQ} (Text S3, Fig. S3).

2.4 Determination of ice cover and lake thermal structure

The model results were used to quantify the fraction of the surface area covered by ice, the depth of the surface mixed layer (SML), i.e. the mixed layer depth *MLD*, and the onset and duration of lake stratification. The fraction of ice coverage was computed as the ratio between the number of surface cells covered by ice to the number of open water surface cells. A winter in which ice covered more than 70% of the lake surface is identified as a “winter with abundant ice cover”, while a winter with smaller ice coverage as a “winter with little ice cover”. The *MLD* was defined as the shallowest depth at which the water density exceeds the density at the lake surface by a prescribed threshold value (Andersen et al., 2017). If the threshold is not exceeded at any depth, the surface mixed layer extends to the lake bottom and *MLD* is equal to the maximum water depth. We used a threshold value of 0.04 kg m^{-3} which is within the range of values used in other studies (Read et al., 2011; Giling et al., 2017). The *MLD* was derived from density profiles, calculated from the simulated temperature using the empirical relations of Chen-

Millero (Chen & Millero, 1986). Prior to the calculation of density, the temperature profiles were linearly interpolated to a vertical resolution of 0.1 m.

The *MLD* was calculated at the deepest location in Gnadensee, i.e. at station M_{GS} (MLD_{GS}), at the deepest location in Zeller See, i.e. at station M_{ZS} (MLD_{ZS}), and at the deepest station along the sill, i.e. at M_{SI} (MLD_{SI}) (Fig. 1e), and along the entire $Trans_{M-R}$ (MLD_S).

The onset of stratification in GS and ZS was defined as the first time in the year at which MLD_{GS} and MLD_{ZS} , respectively, are smaller than the maximum water depth of the corresponding basin. The stratification period of the specific year ended as soon as the mixed layer depth became the maximum water depth of the basin again. Note that inverse temperature stratification can occur during winter at temperatures below 4°C resulting in shallow *MLD*. The time period of inverse temperature stratification is shown in Figs. S4, S6 and Tabs. S2, S3, but was not included as part of the time period referred to as stratified period, which is here restricted to the period with a stratification characterized by decreasing water temperatures with increasing water depth.

2.5 Quantification of the water exchange across the sill between GS and ZS

The model results were used to compute the water exchange across the sill between GS and ZS by analyzing the water flow at 43 stations along $Trans_{M-R}$ (Fig. 1d). The 43 stations were spaced by a regular distance of 74 m. The components of the velocity vector simulated with the model at each of the numerical grid points were interpolated with an inverse distance-weighted method to these 43 stations on $Trans_{M-R}$. This interpolation was conducted for each depth layer separately providing depth profiles of velocities with the same vertical resolution as in the model grid. The velocities at the 43 stations were then expressed in velocity components along and

across the transect Trans_{M-R} . The discharge of water into GS at each of these locations and at each depth layer, $d_{i,j}$, is:

$$d_{i,j} = \text{across_speed}_{i,j} * L * h_j$$

where $i = 1, \dots, 43$ identifies the station along the transect, $j = 1, \dots, N$ the depth layer, N the maximum number of vertical layers, *across_speed* the speed of the velocity component perpendicular to the transect positive into GS, L the distance between the stations and h_j is the vertical height of the depth layer j . The water volume entering (V_{in}) and the water volume leaving (V_{out}) GS per hour were calculated from the sum of all the positive and all negative discharges $d_{i,j}$, respectively. Note that V_{in} and V_{out} were both taken as positive numbers. We characterized water exchange as the total water volume exchanged between neighboring basins per hour, i.e. $V_{exc} = V_{in} + V_{out}$. Annual mean, minimum and maximum water exchange were computed from the time series of V_{exc} . Analogously, we calculated the water exchange above and below the mixed layer depth at Trans_{M-R} , $V_{exc,ML}$ and $V_{exc,B}$, respectively.

The exchange velocity across the sill, v_S , was determined by dividing V_{exc} with the area of the cross-section along Trans_{M-R} above the sill, A_S , i.e. $v_S = V_{exc} / A_S$. According to this definition, the exchange velocity v_S is equivalent to the average magnitude of the velocity component across the sill along Trans_{M-R} , with averaging performed along the transect over the entire water column above the sill. In addition, we calculated analogously the exchange velocity within and below the *SML* at Trans_{M-R} , i.e. above and below the MLD_S ($v_{S,ML}$ and $v_{S,B}$, respectively).

The maximum water depth at the sill, D_S , was determined from the maximum water depth along Trans_{M-R} at station M_{SI} (Fig. 1e). The water level at the sill is denoted as WL_S and WS is the wind speed at a location close to the sill (Fig. 1e, Fig. S8).

2.6 Climate warming scenario

The sensitivity of water temperature, stratification, ice cover, and water exchange to climate warming was assessed by a climate warming scenario assuming an increase in air temperatures by 4°C. This approach is the same as in earlier studies investigating the consequences of climate warming in lakes (Peeters et al., 2007a; Trolle et al., 2011; Kupisch et al., 2012; Straile et al., 2015; Wahl & Peeters 2014) and it is in the range of pessimistic projections of climate warming in the region (IPCC 2014). The climate warming scenario was applied to LLC and to LC. The latter is required to determine the water temperature of Seerhein used as inflow temperature in the corresponding climate warming simulations of LLC (Fig. S1). The water temperature of the other inflows, both for LLC (Radolfzeller Aach) and for ULC, were increased by 95% of the air temperature warming, in accordance to the findings of Michel et al. (2020).

The initial conditions for the warmer climate scenario were derived from a pre-run simulation of LC and LLC in which the model was driven by constructed forcing conditions: the inflow and meteorological conditions of the year 2009 with air temperatures increased by 4°C were repeated three times. The final output of a consecutive simulation of these three years was used as initial condition of the warmer climate simulations. The scenario with air temperature increased by 4°C is denoted as scenario T4 and the reference scenario as scenario T0.

2.7 Water level scenarios

The sensitivity of inter-basin exchange in LLC to changes in water level was investigated based on several scenarios with altered water levels. Two scenarios, referred to as “fixed-shift water-level scenarios”, assume that the water level is at all times 30 cm higher (W+), or 30 cm

lower (W_-) respectively, than in the reference scenario T0. Additionally, four “seasonal water level scenarios” were considered: Scenario W_m assumes a seasonal course of water level that corresponds to the mean seasonal course of water level over the last 200 years measured at station Berlingen in LLC (Luft & van den Eertwegh, 1991). The scenario W_{m+} assumes a 30 cm higher and W_{m-} a 30 cm lower water level than W_m at all times. W_{m+} and W_{m-} are thus analogous to scenarios W^+ and W^- but refer to W_m as reference scenario. The scenario $W_{m,w+s-}$ assumes a 30 cm higher minimum water level in winter and a 30 cm lower maximum water level in summer than W_m . The transition between winter and summer water level is represented by a spline (Fig. S15). The latter scenario assumes a seasonal course of water level along the lines of the expectations for a warmer climate (Ostendorp et al., 2020). In a warmer climate less snow will be stored in the catchment of ULC during winter and snowmelt in spring will therefore provide less water than today. Hence, compared to the water levels in ULC and LLC today, water levels in a warmer climate are expected to be higher in winter and lower in summer resulting in a reduced amplitude of the seasonal water level dynamics (Ostendorp et al., 2020).

In all water level scenarios, the meteorological conditions were the same as in T0, but inflow and outflow conditions were adjusted to match the seasonal course of water level of the respective water level scenario considering the relation between water level and output discharge obtained from the water balance of the field observations.

Simulations of W^+ and W^- covered the entire time period from 2009 to 2018, whereas simulations of the seasonal water level scenarios W_m , W_{m+} , W_{m-} , and $W_{m,w+s-}$ focused on two years with very different ice coverage, i.e. November 2009 – December 2010 (abundant ice cover) and November 2015 – December 2016 (little ice cover).

2.8 Analysis of the simulation results with respect to the seasonal pattern of V_{exc} and the impact of climate warming and water level changes

The identification of seasonal patterns and the impact of climate warming and water level changes is based on monthly averages of V_{exc} , v_S , WL_S , D_S , MLD_{SI} , A_S , and WS . Potential links between the seasonal change of these parameters during the open water period were assessed using linear regression. This analysis was performed using monthly-mean data averaged over the years 2010 to 2017 considering only the ice-free period, i.e. all month between April and December. The multi-annual averages of monthly-mean values are denoted by the subscript m . The impact of climate warming and water level change was assessed by determining the difference between the results obtained with the scenario considering changing conditions (scenario T4, W+ or W-) minus the results from the reference scenario T0. The focus was on a comparison of monthly-mean V_{exc} , ΔV_{exc} , and monthly-mean v_S , Δv_S , respectively, but changes in other parameters were also considered. These monthly mean differences were additionally averaged over all years providing e.g. $\Delta V_{exc,m}$ and $\Delta v_{S,m}$ and additional multi-annual means of monthly mean properties.

2.9 Tracer experiments

A numerical tracer experiment was conducted with AEM3D to investigate the spreading of water from river Seerhein along transect $Trans_{I-G}$ into GS. Between January 2010 and December 2017 each month a tracer was introduced continuously from river Seerhein by assigning a constant concentration of 1 mg m^{-3} to the inflowing water. At the end of each month the tracer concentration in the entire lake was set to zero to provide initial conditions (regarding the tracer concentration) for the following month or for the different scenarios of the same

month. This experiment was conducted for the reference scenario T0, the climate warming scenario T4 and the water level scenarios W₊ and W₋.

Monthly snapshots of the concentration distribution of the tracer along Tans_{G-I} were taken 2 days after the beginning of each month to illustrate the transport of the tracer towards GS in the year 2010 (Figs. S17-S20). Moreover, from the model output we computed the time series of tracer mass in GS ($M_{TR,GS}$) and of the tracer mass introduced in the lake (M_{TR}). Hence, the fraction of tracer mass introduced by river Seerhein reaching GS was defined as $m_{TR} = M_{TR,GS}/M_{TR}$. The time series of m_{TR} provides information on the time required of tracer to reach GS. The m_{TR} 25 days after the first introduction of the tracer in the respective month was indicated as $m_{TR,25}$.

3 Results

3.1 Temporal patterns of stratification, ice cover, currents, and water exchange

Under reference conditions (scenario T0) in all of the nine years simulated (March 2009-March 2018) stable stratification established between spring and fall in all basins of LLC. In GS stable stratification started between the 77th day (day of the year) and the 104th day and lasted about 7-8 months (Figs. 2, S4, Tab. S2). In ZS, onset of stratification occurred on average 1 day earlier and duration of stratification was on average 15 days shorter than in GS (Fig. S6, Tab. S3). In all simulated years, at least partial ice cover developed in LLC during winter (Fig. 2). Substantial ice cover occurred in all basins of LLC in 2010, 2011, 2012, 2015 and 2017, whereas in the other years, ice cover developed only in GS. Freezing typically occurred between January and March, but extent and duration of the ice coverage showed a pronounced inter-annual variability (Fig. 2). During periods with ice cover, inverse stratification developed in the

uppermost 1-2 m of the water column (Figs. S4, S6). Monthly mean ice cover of more than 30% only occurred during months in winter (January to March). Between April and December all months in all years had average ice cover less than 30% of the lake surface, and this time-period of the year is therefore considered as the ice-free season.

Caramatti et al. (2020) have already shown that the model simulations of stratification and ice cover in LLC are in good agreement with observations (Text S2, Fig. S2, Tab. S1). Also simulated and observed current speeds at station M_{AQ} on the sill agree well with respect to the seasonal pattern, to the differences between stratified and mixed periods, and to the timing of high and low current speeds (Fig. S3). The comparison between measured and simulated velocity components across and along the transect $Trans_{M-R}$ indicated a RMSE of 1.0 cm s^{-1} and 0.5 cm s^{-1} , respectively, which is partially due to phase shifts in the time series and comparable with RMSE observed in other studies modelling the hydrodynamics in lakes (Nguyen et al. 2017; Dissanayake et al. 2019).

The simulated inter-basin water exchange showed a pronounced seasonal pattern characterized by higher water exchange during summer than during winter (Fig. 2a). The annual maximum exchange typically occurred between June and July and ranged between 11.6×10^5 and $20.0 \times 10^5 \text{ m}^3 \text{ h}^{-1}$. The annual minimum exchange, ranging between 1.3×10^5 and $4.0 \times 10^5 \text{ m}^3 \text{ h}^{-1}$, occurred between February and March and was lowest in years with the largest ice coverage (year: 2010, 2011, 2012, 2015 and 2016 in Fig. 2a). Shortly before the development of ice cover, water exchange typically exhibited a secondary peak (Fig. 2a) which occurred at the same time as a corresponding secondary peak in water level (Fig. 2b). The amplitude and the details of the seasonal pattern of water exchange, and also the annual mean water exchange varied between years (Fig. 2a).

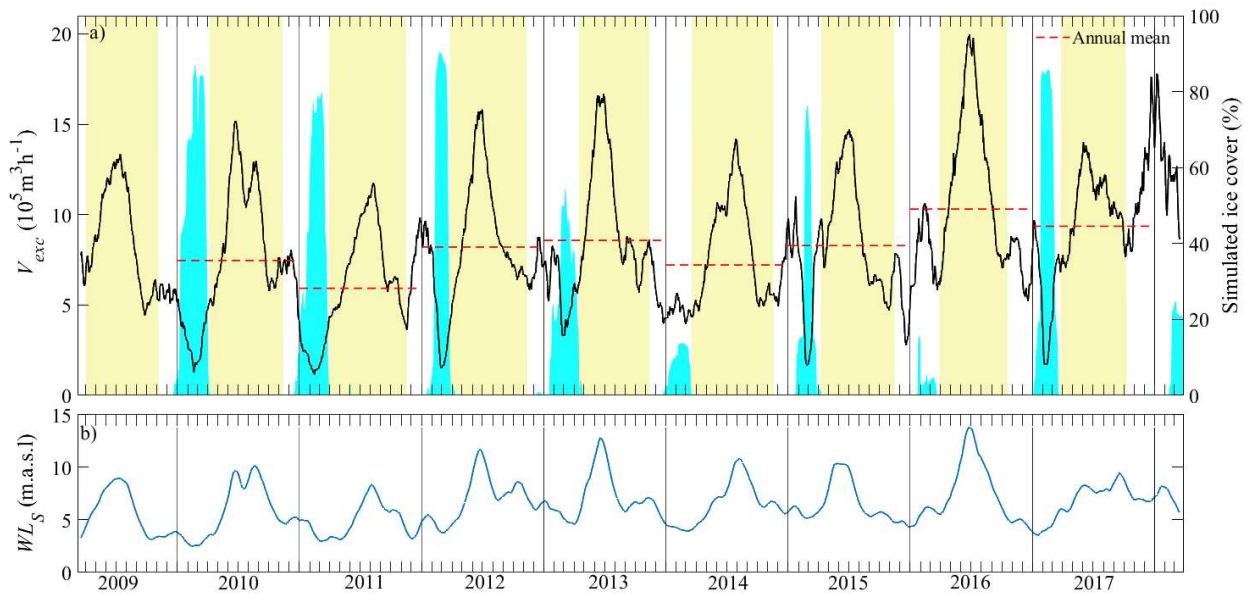


Figure 2: Simulated water exchange (V_{exc}) across the Trans_{M-R} and water level (WL_S) between 2009 and 2018. The time series of hourly water exchange and water level were smoothed using a 30 days running mean. The annual mean water exchange is indicated by a red dashed line. The duration of the stratification period at M_{GS} is shaded in yellow, while the simulated percentage of lake surface covered by ice is shaded in cyan.

3.2 Relation between seasonal pattern in water exchange and other seasonally-varying parameters

The seasonal pattern of water exchange V_{exc} was compared to the seasonal change of v_S , WL_S , A_S , MLD_{SI} , and WS (Fig. 3). The seasonal course of V_{exc} , v_S , WL_S , and A_S was characterized by high values in summer and low values in winter. MLD_{SI} , however, was shallow in summer and progressively increased until it reached the maximum depth of the sill in November and December (Fig. 3f). During winters with little ice cover MLD_{SI} remained large until spring, whereas it was 2 m or shallower in ice-covered months due to inverse stratification below the

ice. In contrast to all other parameters considered above, wind speed and wind direction, WS and wind direction, WD , did not show a seasonal pattern but remained rather constant throughout the year (Figs. 3i, S9).

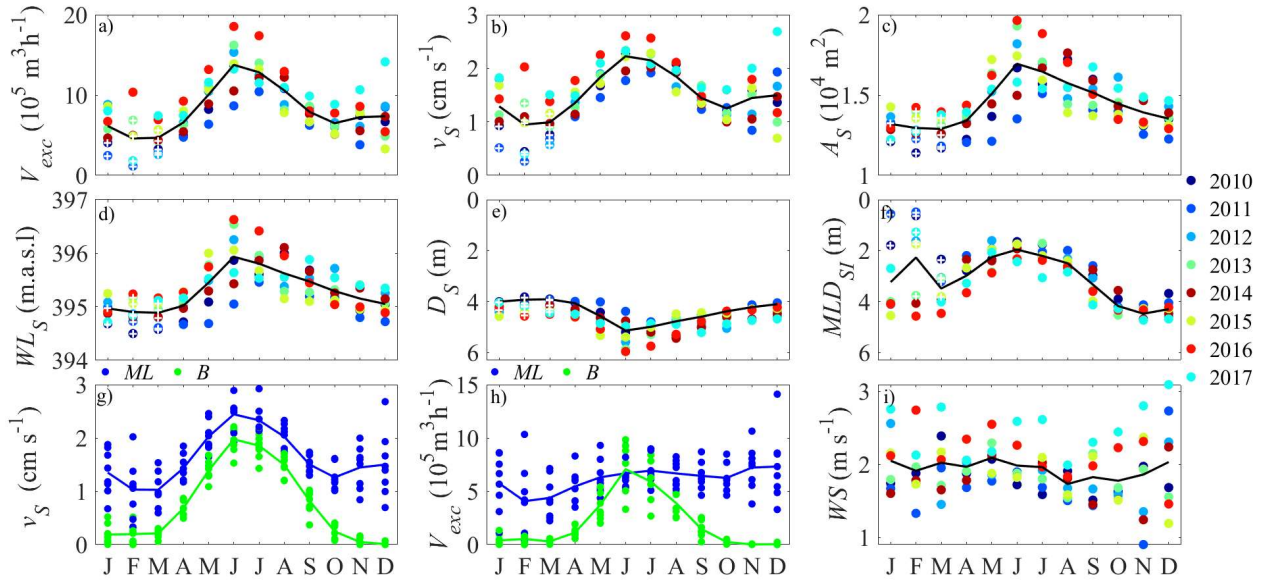


Figure 3: Seasonal pattern of water exchange V_{exc} and additional parameters relevant for the exchange across the sill. Seasonal pattern of a) V_{exc} , b) average current speed across $Trans_{M-R}$, v_S , c) area of the cross-section above the sill along of $Trans_{M-R}$, A_S , d) lake water level, WL_S , e) maximum depth along $Trans_{M-R}$, D_S , f) mixed layer depth at the deepest station of $Trans_{M-R}$, MLD_{SI} , g) seasonal pattern of the average current speed within and below the mixed layer along $Trans_{M-R}$ (MLD_S), $v_{S,ML}$ and $v_{S,B}$, respectively, h) seasonal pattern of the water exchange above and below MLD_S , $V_{exc,ML}$, and $V_{exc,B}$, respectively, and i) wind speed WS close to the sill. The symbols represent the monthly-averaged quantity for each year. The black line connects the multi-annual average of the monthly values (years 2010 – 2017). The months with a monthly-mean ice cover above 30% of the lake surface are identified by a white “+”.

Statistical analysis confirms a highly significant positive correlation between the multi-annual average (2010-2017) of the monthly-mean water exchange, $V_{exc,m}$, and the corresponding $v_{S,m}$, WLS_m , and AS_m (Tab. S5), whereas $V_{exc,m}$ is not significantly correlated with $MLD_{SI,m}$ ($p = 0.06$). Considering only the ice-free season, the correlations between $V_{exc,m}$ and WLS_m , AS_m , and $v_{S,m}$ (Fig. 4a-c), are similar as in the analysis based on all seasons, but additionally, $V_{exc,m}$ and $MLD_{SI,m}$ are significantly anti-correlated (Fig. 4d, Tab. S4). During the ice free season $v_{S,m}$ correlates similarly well with WLS_m , AS_m , and $MLD_{SI,m}$ as $V_{exc,m}$. E.g., $v_{S,m}$ is significantly correlated to WLS_m ($r = 0.88$, $p < 0.001$) and significantly anti-correlated to $MLD_{SI,m}$ ($r = -0.82$, $p = 0.01$) (Fig. 4e-f, Tab. S4). However, neither $V_{exc,m}$ nor $v_{S,m}$ are significantly correlated to WS_m ($p \geq 0.4$ in both cases, Fig. 4j-k, Tab. S4). Because the seasonal change in AS is a direct consequence of the seasonal water level change, WLS_m explains essentially the entire variance of AS_m ($R^2 = 1.00$, Fig. 4i), and correlations of the other parameters with WLS_m and AS_m provide the same results for r and p .

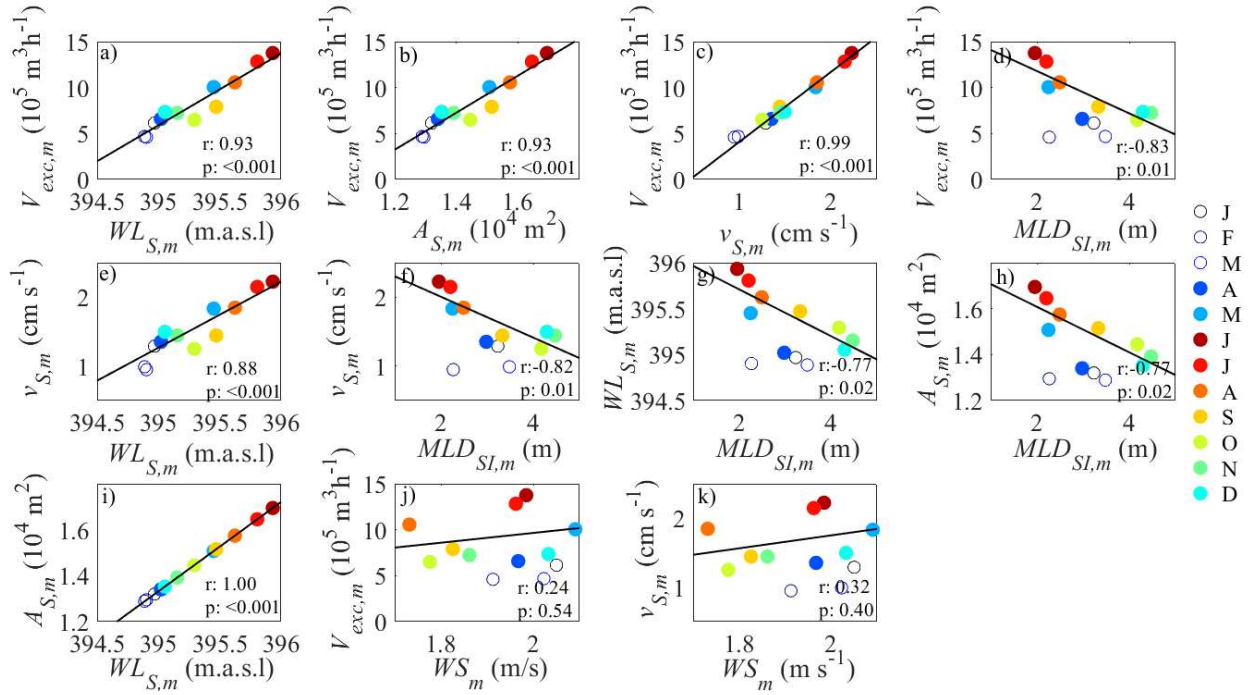


Figure 4: Correlations between the seasonal change of water exchange V_{exc} and other parameters relevant for water exchange at the sill. The symbols represent the simulated multi-annual averages (years 2010 – 2017) of the monthly-mean properties water exchange $V_{exc,m}$, water level $WL_{S,m}$, area of the cross-section along Trans_{M-R} above the sill $A_{S,m}$, current speed across Trans_{M-R} , $v_{s,m}$, mixed layer depth at the station M_{SI} , $MLD_{SI,m}$, and wind speed close to the sill WS_m . Open circles indicate values for ice-covered months (January – March) that were not included in the regression analysis. The black line is the regression line. An overview on the statistical results of the linear regression analysis is provided in Tab. S4.

The exchange velocity across the sill was always substantially larger within the SML than below the SML (v_{S_ML} and v_{S_B} , Fig. 3g). Both, v_{S_ML} and v_{S_B} , showed a clear seasonal pattern with largest values in summer and smallest in winter and fall. The water exchange, however, followed a similar seasonal pattern only below the SML but not within the SML

(V_{exc_ML} and V_{exc_B} Fig. 3h). Note, that v_{S_B} and V_{exc_B} become zero when MLD reaches the water depths D_S at the sill. During the ice-free season $v_{S_B,m}$, $v_{S_ML,m}$, and $V_{exc_B,m}$ were significantly anti-correlated to $MLD_{SI,m}$ ($r = -0.92, p < 0.001, r = -0.87, p < 0.001, r = -0.92, p < 0.001$, respectively; Tab. S4-S5) whereas the correlation between $V_{exc_ML,m}$ and $MLD_{SI,m}$ was positive and not significant ($r = 0.28, p = 0.47$).

Seasonal water level changes not only affect the seasonal course of V_{exc} , but also that of v_s (Fig. S13). In a model run in which the outflow was adjusted to provide a constant water level from April until December, i.e. in which the water level in summer and fall was lower than in scenario T0, v_s is lower than in scenario T0. This result suggests that at lower water level the average frictional effect resulting from the interaction between currents and bottom boundary at the sill become larger.

In the open water at the deepest stations in GS and ZS, monthly mean vertical profiles showed a pronounced seasonal change in the vertical distribution of current speed (Fig. S10a-b). In the depth range from the surface down to the maximum depth of the sill current speed was almost uniform in July but decreased strongly with depth in December. In December currents were typically larger than in July. At the deepest station on the sill, M_{SI} , the vertical distribution of the monthly mean current speed was similar to that in the open water, but current speeds in July were larger than at M_{GS} and M_{ZS} (Fig. S10c). The monthly mean speed of the current across the sill was larger in July than in December and decreased only slightly with depth in both months (Fig. S10d).

The vertical averages of the monthly mean current speed from the surface down to D_S at M_{GS} , M_{ZS} , and M_{SI} showed a seasonal pattern during the ice-free period that was similar to that of v_s (Fig. S10, Fig. 3b), i.e. an increase between April and July and a decrease from July to

October. From October onwards, the increase of the vertically averaged open water current speeds (Fig. S10e-f) was similar to that of the vertically averaged current speed at the sill (Fig. S10g), but more pronounced than the increase of the average speed of the current across the sill (Fig. S10h) and of the exchange velocity v_S (Fig. 3b).

3.3 Impact of a warmer climate on ice cover, stratification, and water exchange

In a warmer climate, characterized here by a 4°C increase in air temperature (scenario T4), all basins in LLC will be ice-free in all years. Therefore, inverse stratification did never develop in scenario T4 (Figs. S5, S7) and MLD_{SI} during January and February and in months in March that were ice covered in scenario T0 was always larger than in the reference scenario T0 (Fig. 5c,f). In scenario T4, the onset of spring/summer stratification in GS and ZS was on average shifted forwards in time by 18 and 20 days, respectively, and the duration of stratification increased on average by 34 and 42 days, respectively (Tabs. S2—S3). In April and May MLD_{SI} was shallower in scenario T4 than in scenario T0 whereas in summer and fall the absolute change in MLD_{SI} was small (Fig. 5c,f). In November and December $\Delta MLD_{SI} = 0$ because in scenario T0 and T4 the SML extends down to the maximum depth of the sill.

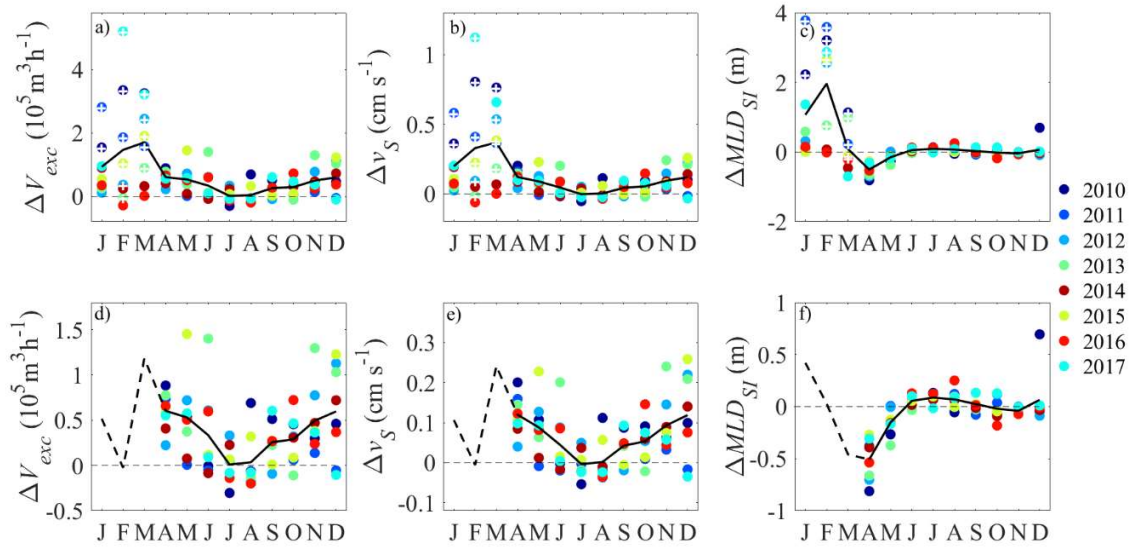


Figure 5: The impact of climate warming on water exchange, exchange velocity across the sill and mixed layer depth. Climate warming induced changes were determined from the monthly mean difference between the value of the parameters determined in scenario T4 minus its value in scenario T0. Depicted is the change in the monthly mean a) water exchange ΔV_{exc} , b) speed of the current across the sill Δv_S and c) MLD_{SI} (ΔMLD_{SI}). Panels d-f depict the corresponding parameters considering only the ice free season which allowed for a different scaling. The symbols represent monthly-averaged quantities in the years 2010-2017. The solid black line connects multi-annual averages, the dotted line connects multi-annual averages considering only ice-free month.

In years with abundant ice cover under reference conditions water exchange between January and March was substantially larger in scenario T4 than in T0 (ΔV_{exc} up to $5.2 \times 10^5 \text{ m}^3 \text{ h}^{-1}$, Fig. 5a,d). During the ice free season, the main increase in water exchange occurred in spring

(March – May) and also in late fall (November – December), but during the summer months ΔV_{exc} was close to zero (Fig. 5a,d).

Similar to V_{exc} , the exchange velocity v_s was typically larger in scenario T4 than in T0. Δv_s was particularly large during winter months, which were ice covered in scenario T0 (Fig. 5b,e). During the ice-free season v_s was larger in scenario T4 compared to scenario T0 especially in spring and late fall, whereas v_s remained essentially the same in both scenarios during the summer months (Figs. 5b, 5e).

During the ice-free season, the changes of V_{exc} and v_s , and of the corresponding properties within and below the SML, caused by climate warming, were linked to the change of MLD.

ΔV_{exc} , $\Delta V_{exc,B}$, Δv_s , $\Delta v_{s,ML}$, $\Delta v_{s,B}$ were significantly anti-correlated to ΔMLD_{SI} (Tab. S6). Only $\Delta V_{exc,ML}$ showed a positive correlation to ΔMLD_{SI} which however was not significant (Tab. S6).

3.4 Impact of water level on ice cover, stratification, and water exchange

At the reduced water levels assumed in scenario W- the surface area covered by ice in winter was typically larger than at the increased water levels assumed in scenario W+ (Fig. S14). Nevertheless, the timing of ice-on and ice-off did not differ significantly between scenarios T0, W+, and W-. Also the onset, duration and strength of stratification was essentially the same in these three scenarios, i.e. monthly mean MLD_{SI} differed by less than 1.2 m between scenarios in all years and months, beside January 2011 for the scenario W+ (Fig. 6c,f).

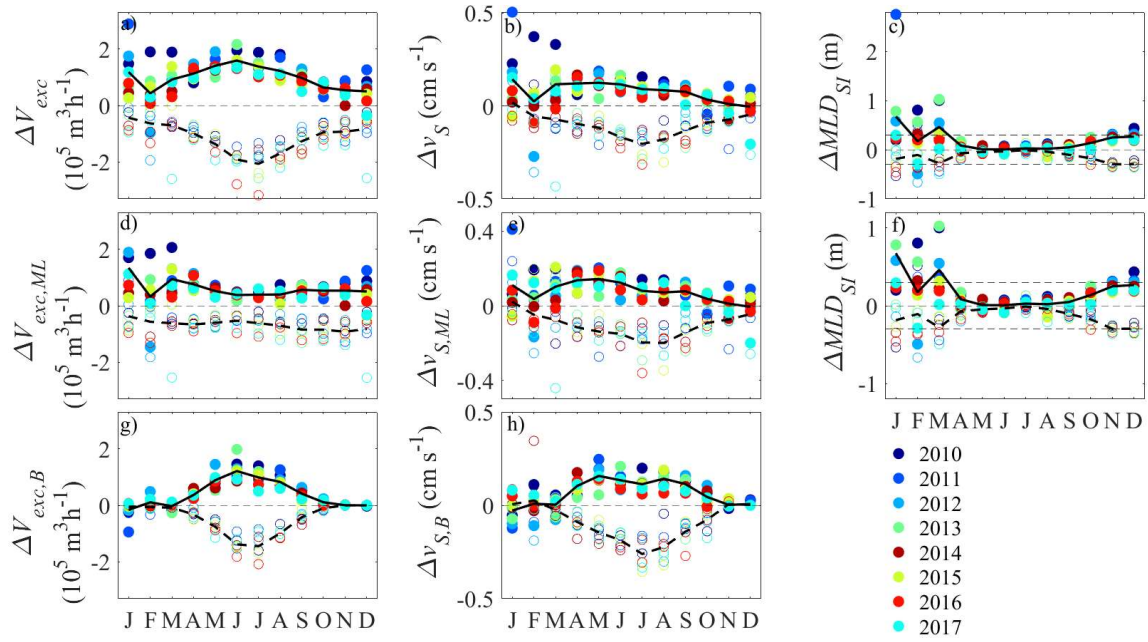


Figure 6: The impact of water level change (scenarios W+ and W-) on water exchange, exchange velocity across the sill and mixed layer depth. The panels depict the change of a) water exchange, ΔV_{exc} , considering the entire cross-section above the sill along $Trans_{M-R}$, d) water exchange above the MLD_S , $\Delta V_{exc,ML}$, and g) water exchange below the MLD_S , $\Delta V_{exc,B}$. The change of the mean speed of the current across the sill b) averaged over the entire cross-section between the basins, Δv_S , e) above the MLD_S , $\Delta v_{S,ML}$, and h) below the MLD_S , $\Delta v_{S,B}$. c) and f) The change in the mean layer depth at the station M_{SI} (ΔMLD_{SI}). The changes of the different properties, Δ are the monthly mean differences between the value of the property determined in scenario W+ and W-, respectively, minus its value in scenario T0. The symbols represent monthly-averaged quantities in the years 2010-2017. The solid black line connects multi-annual averages for the scenario W+, while the dashed black line connects multi-annual averages for W-.

Compared to scenario T0, V_{exc} increased in scenario W+ and decreased in scenario W- (Fig. 6a). The change in V_{exc} for the two water level scenarios is partially caused by the change in

the area of the cross-section along $\text{Trans}_{\text{M-R}}$ above the sill: in scenario W^+ A_S is larger and in scenario W^- smaller than in scenario T0 . However, not only V_{exc} and A_S but also v_s was larger in scenario W^+ than in scenario T0 (Fig. 6b), although stratification did not change substantially. The increase in V_{exc} and v_s in scenario W^+ compared to scenario T0 was largest during summer and smallest in winter. In scenario W^- not only ΔV_{exc} but also Δv_s was negative. In scenario W^- the absolute values of ΔV_{exc} and Δv_s had a similar seasonality as in scenario W^+ but were larger than in scenario W^+ .

The seasonal pattern of the impact of water level change on water exchange and current speed across the sill is dominated by the seasonal pattern of the changes below the SML, $\Delta V_{exc,B}$ and $\Delta v_{s,B}$ (Fig. 6g-h). The seasonal pattern of the changes of ΔV_{exc} and Δv_s within the SML, $\Delta V_{exc,ML}$ and $\Delta v_{s,ML}$, respectively, were weaker as those of $\Delta V_{exc,B}$ and $\Delta v_{s,B}$ (Fig. 6d-g). Future projections of the water level of Lake Constance suggest that water level change will be characterized by a reduced seasonal amplitude of the water level, i.e. higher levels in winter and lower levels in summer (scenario $\text{W}_{\text{m,w+s}}$). In comparison to scenario W_{m} , that uses the average long term seasonal change of the water level, the simulations with scenario $\text{W}_{\text{m,w+s}}$ predicted stronger inter-basin exchange during winter and reduced exchange during summer (Fig. 7). The annual mean impact of the water level change on water exchange assumed in scenario $\text{W}_{\text{m,w+s}}$ was smaller than that of the water level changes assumed in scenario W_{m^+} and W_{m^-} and opposite between the year with abundant and the year with little ice cover (Fig. 7b,d).

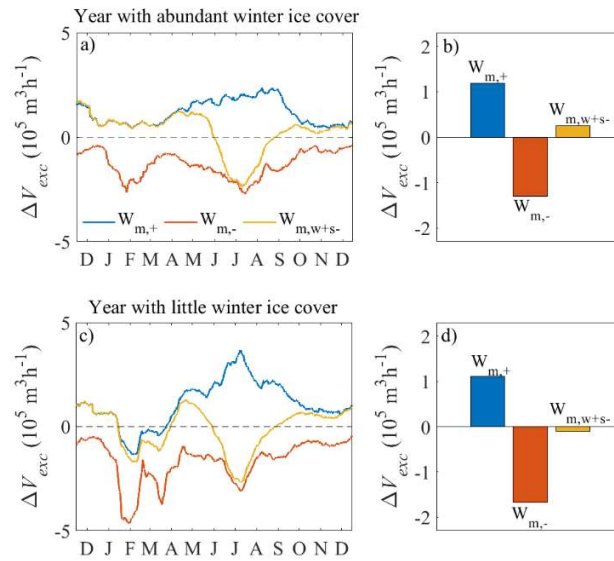


Figure 7: Impact of seasonally non-uniform changes in water level on water exchange V_{exc} . ΔV_{exc} is the difference between V_{exc} in the “seasonal water level scenarios” $W_{m,-}$, $W_{m,+}$, $W_{m,w+s}$ and scenario W_m . W_m assumes water levels that correspond to the multi-annual average seasonal course of the water level over the last 200 years (measured in LLC). $W_{m,w+s}$ assumes 0.3 m higher water levels during the winter months and 0.3 m lower water levels during summer months than in W_m . Scenarios $W_{m,+}$ and $W_{m,-}$ assume a constant increase and decrease of the water level by 0.3 m, respectively. The time series of ΔV_{exc} is shown for the time period a) November 2009 – December 2010, as representative for years with abundant winter ice cover, and c) November 2015 – December 2016, as representative for years with little winter ice cover. Annual averages of ΔV_{exc} are provided b) for November 2009 – December 2010 and d) for November 2015 – December 2016.

3.5 Transport of dissolved substance from the main inflow to GS

Dissolved substances introduced into LLC by river Seerhein are transported from its mouth in RS via ZS to GS (Fig. S17). The vertical distribution of the tracer along Trans_{I-G} changed substantially during the season in 2010. Two days after the introduction of the tracer at Seerhein, tracer was vertically mixed in RS before reaching GS during the winter months, whereas between May and October the tracer concentrations were maximal within the thermocline of RS and ZS (Fig. S17e-j). However, only in July and August 2010 tracer concentrations above the sill between ZS and GS were high (Fig. S17g-h). The tracer mass reaching GS within one month was substantially lower during winter than in summer (Fig. 8a). The seasonal pattern of the fractionation of tracer mass introduced by Seerhein reaching GS (Fig. 8a) was positively correlated to WL_S ($r = 0.55$, $p < 0.001$) and to the average MLH_{I-G} ($r = 0.37$, $p < 0.001$). Between June and September $m_{TR,25}$ was larger than in spring and winter (Fig 8) indicating a higher connectivity of surface water between inflow in RS, ZS and GS. Furthermore, in June and September a larger fraction of the river water reached GS faster than in spring and winter, as is indicated by the comparatively rapid increase of m_{TR} in these months (Fig. S22).

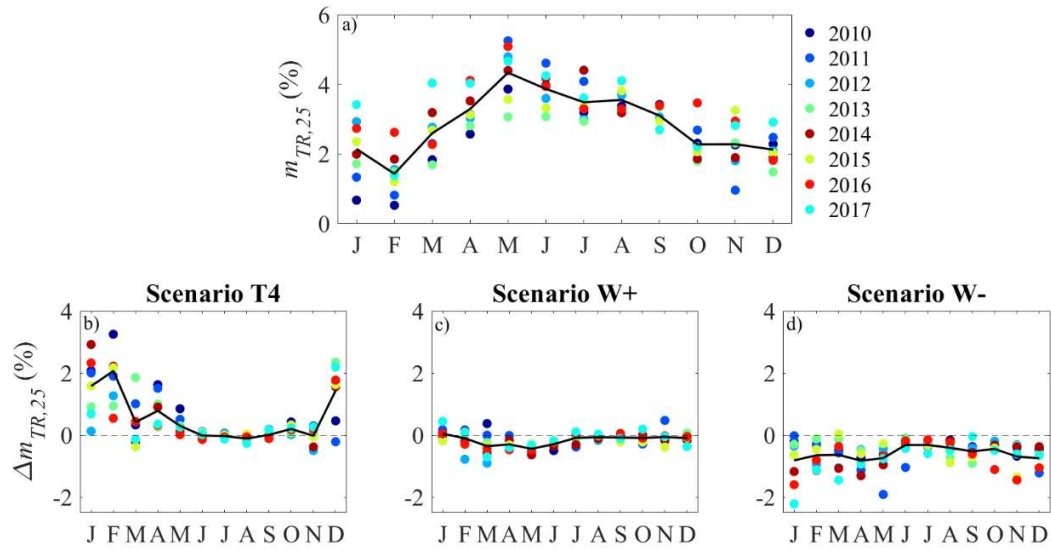


Figure 8: Seasonal pattern of the fraction of tracer mass introduced by river Seerhein reaching GS, $m_{TR,25}$, (a) and the impact of climate warming and water level change (b-d). Panels (b) to (d) depict monthly changes in $m_{TR,25}$, $\Delta m_{TR,25}$, that are caused by the scenarios T4, W+ and W-, respectively.

In a warmer climate (scenario T4) substantially more tracer reached GS in winter and late fall than under current conditions (scenario T0) (Fig. 8b). E.g. in January and February the tracer mass transported into GS in scenario T4 is typically twice as large as in the reference scenario T0 and the increase of $m_{TR,25}$ between scenarios T4 and T0, $\Delta m_{TR,25}$, can be more than 600% larger than $m_{TR,25}$ under reference conditions (February 2010: $m_{TR,25} = 0.53\%$ and $\Delta m_{TR,25} = 3.3\%$). In contrast, climate warming has essentially no effect on the connectivity between river Seerhein and GS during summer. A seasonally constant water level change as in the scenarios W+ and W- results in a comparatively small impact on the tracer mass reaching GS (Fig. 8c-d).

4 Discussion

4.1 Inter-basin exchange in LLC: Controlling factors

The identification of the main drivers controlling seasonal and inter-annual changes in inter-basin exchange in lakes with complex morphometry is important for the understanding of spatial heterogeneities in the distributions of dissolved substances and organisms and for the assessment of the potential impact of climatic and hydrological changes on these distributions.

The numerical simulations revealed a strong seasonal pattern in the inter-basin exchange between GS and ZS. The seasonal change in $V_{exc,m}$ results from two effects: a) the change in the exchange velocity across the sill between GS and ZS and b) the change in the area of the cross-section through which water flows across the sill:

$$\delta V_{exc,m} = \delta v_{S,m} \cdot A_{S,m,r} + v_{S,m,r} \cdot \delta A_{S,m} + \delta v_{S,m} \cdot \delta A_{S,m}$$

where $\delta V_{exc,m} = V_{exc,m} - V_{exc,m,r}$, $\delta v_{S,m} = v_{S,m} - v_{S,m,r}$, and $\delta A_{S,m} = A_{S,m} - A_{S,m,r}$, and $V_{exc,m,r}$, $v_{S,m,r}$, and $A_{S,m,r}$ are $V_{exc,m}$, $A_{S,m}$ and $v_{S,m}$ at a reference month. The contribution of $\delta v_{S,m}$ to the seasonal change in water exchange, $\delta v_{S,m} \cdot A_{S,m,r}$, is typically larger than the contribution to $\delta V_{exc,m}$ due to the change in $A_{S,m}$, $v_{S,m,r} \cdot \delta A_{S,m}$. The correlation of the changes in $v_{S,m}$ and $A_{S,m}$, $\delta v_{S,m} \cdot \delta A_{S,m}$, has only a very small influence on $\delta V_{exc,m}$ (Fig. 9).

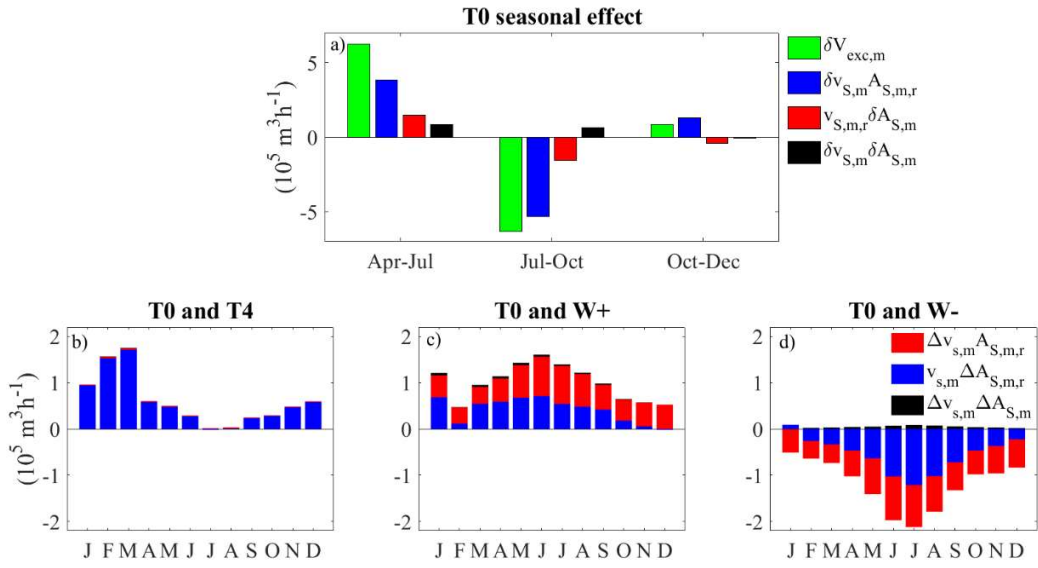


Figure 9: The contributions of exchange velocity and the cross-sectional area above the sill to the change in the exchange velocity. (a) Seasonal changes of $V_{exc,m}$ in scenario T0, $\delta V_{exc,m}$, and the contribution to $\delta V_{exc,m}$ of the seasonal change in the exchange velocity, $\delta v_{s,m}$, and in the cross sectional area above the sill, $\delta A_{s,m}$: $\delta V_{exc,m} = \delta v_{s,m} \cdot A_{s,m,r} + v_{s,m,r} \cdot \delta A_{s,m} + \delta v_{s,m} \cdot \delta A_{s,m}$. $v_{s,m,r}$ and $A_{s,m,r}$ are $A_{s,m}$ and $v_{s,m}$ at the reference months April, July, and October, respectively. (b-d) The contribution of $v_{s,m}$ and $A_{s,m}$ to changes in $V_{exc,m}$ resulting from warming (b: Scenario T4) and water level changes (c: Scenarios W+ ; d: Scenario W-): $\Delta V_{exc,m} = \Delta v_{s,m} \cdot A_{s,m,r} + v_{s,m,r} \cdot \Delta A_{s,m} + \Delta v_{s,m} \cdot \Delta A_{s,m}$. Δ denotes the difference between a property in T4, W+, or W- minus its value in reference scenario T0 in the corresponding month. $A_{s,m,r}$ and $v_{s,m,r}$ are the values of $A_{s,m}$ and $v_{s,m}$ in the reference scenario T0.

During the ice-free period, $\delta v_{s,m} \cdot A_{s,m,r}$ was typically more than two times larger than $v_{s,m,r} \cdot \delta A_{s,m}$, e.g., from April to July and from July to October the change in the average current speed across the sill accounts for more than 70% of the increase and decrease, respectively, of

the water exchange $V_{exc,m}$ (Fig. 9a). Between October and December, $v_{S,m}$ increased and $A_{S,m}$ decreased, but because the absolute value of $\delta v_{S,m} \cdot A_{S,m,r}$ was about two times larger than the absolute value of $v_{S,m} \cdot \delta A_{S,m,r}$, $V_{exc,m}$ increased (Fig. 9a).

Since the seasonal change of $V_{exc,m}$ results from the seasonal change in $A_{S,m}$ and $v_{S,m}$, it is controlled by the factors determining $A_{S,m}$ and $v_{S,m}$. The seasonal change in $A_{S,m}$ is proportional to the seasonal change in water level (Fig. 3d) and hence determined by the hydrology in the catchments, i.e. by the inflows and outflows of the lake system. The seasonal change in $v_{S,m}$ results from the complex interaction between wind forcing, stratification, and water level affecting the vertical distribution of currents. Furthermore, $v_{S,m}$ is influenced by bottom friction, which depends on morphometry and water level at the sill (Fig. S13).

Wind speed and wind speed squared, which is proportional to forcing at the lake surface, remained rather constant over the season (Fig. S9). Thus, the seasonal course in $v_{S,m}$, and also of the current speed at the deepest stations in GS and ZS and at the sill, are not caused by the seasonal changes in wind forcing, but connected to the seasonal change in stratification, here indicated by the seasonal change in MLD, and in water level affecting friction.

Between April and October, $v_{S,m}$ and the vertical average of the current speed at M_{GS} and M_{ZS} in the upper part of the water column (down to the depth of the sill) are larger at shallower and smaller at larger MLD (Figs. 3b and S10). Apparently, the efficiency of the transfer of wind energy to kinetic energy in the horizontal current field in the upper ~5 m of the water column increases with increasing stratification. Stratification suppresses vertical motion and thus less of the kinetic energy transferred by wind forcing to horizontal motions may be lost to vertical motions and turbulence (Bennett, 1974). Furthermore, stratification supports internal seiching that channels wind energy into oscillatory motions of the entire water column and thus may

support larger horizontal current speeds by enhancing energy transfer from wind to water. The vertical distribution of the current speed in summer at M_{GS} and M_{ZS} (Fig. S10) suggest the impact of seiching, as the current speed does not decrease much with depth but remains rather constant. Indeed, the velocity profiles at M_{GS} and M_{ZS} show strong opposing currents within the upper 5 m that change periodically with time (Fig. S12).

From October to December current speeds at M_{GS} , M_{ZS} and M_{SI} increase, while the lake is essentially fully mixed in November and December (Fig. S10). Monthly mean vertical profiles of current speed at M_{GS} and M_{ZS} show a larger but rather monotonous decrease from the surface to larger depth than summer profiles. In this period, a large portion of the water column in the open water moves synchronously in one direction. The inertia of this water body supports more continuous flow throughout the water column by reducing the influence of changing directions of wind forcing. During stratified conditions in summer, the currents move instead in opposite directions within and below the SML (Fig. S11) as a consequence of seiching. Hence, during unstratified conditions, the losses by friction within the water column are reduced, resulting in increased wind driven current speeds. Also in Lake Erie strong wind-driven currents were the cause for large inter-basin exchange during unstratified conditions (Niu et al., 2015).

With shallowing of the MLD in summer, the exchange velocity within and below the SML increased (Fig. 3g). However, despite the seasonal increase of $v_{s,ML}$, $V_{exc,ML}$ did not show a strong seasonal pattern, because the shallowing of the MLD in summer is associated with a decrease of the area of the cross-section available for water exchange within the SML. The decrease in cross-sectional area of the SML apparently compensated the increase of $v_{s,ML}$. The seasonal change in V_{exc} was therefore dominated by the seasonal change in $V_{ex,B}$, which was a consequence of the combined effect of the seasonal change in $v_{s,B}$ and the seasonal increase in

the cross-sectional area at the sill below the SML. The latter resulted from the decrease in MLD and additionally from the seasonal increase in water level.

The exchange velocity below the MLD increases more strongly than the exchange velocity within the SML (Fig. 3g). At same water depth, the shallower MLD the more currents from a larger distance to the bottom of the sill are included in the estimate of $v_{s,B}$. This may explain the comparatively large change in $v_{s,B}$ with decreasing MLD, because the effect of bottom friction on the current speed decreases with the distance to the bottom.

The scenario with constant water level in summer revealed that the seasonal increase in water level contributed to the increase of the overall exchange velocity v_s (Fig. S13). This result suggests that at higher lake water level the impact of bottom friction on average currents is reduced (Gregg, 2004; Rueda & Cowen, 2005) and that water level changes therefore have an indirect impact on the seasonal change of V_{exc} by altering the effects of bottom friction. Summarizing for the open water period, the seasonal changes in v_s , $v_{s,ML}$, and $v_{s,B}$ result from I) seasonal changes in the efficiency of the energy transfer from wind forcing to horizontal water currents, II) seasonal changes in water level affecting the impact of friction on the current speed at the sill, and III) seasonal changes in cross-section available for exchange-

The formation or absence of ice is independently affecting water exchange causing high inter-annual variability of water exchange during winter months. The ice layer inhibits the transfer of wind energy to the water at the lake surface and thus leads to reduced horizontal current speeds and smaller inter-basin exchange (Fujisaki et al., 2013; Nguyen et al., 2017). Inter-basin exchange can therefore differ substantially between winters with the same water level but different ice coverage (Figs. 2a and 3a). However, the annual mean exchange is not necessarily larger in years with little winter ice cover than in years with abundant winter ice

cover (Fig. 2) because water exchange is largest during the summer months, which compensates for low exchange during ice covered winters.

The spread of the river inflow into GS is affected by lake thermal structure (Fig. S17). In summer, river Seerhein intruded as density plume into the metalimnion of RS and ZS as its typical for river inflows during the stratified season (Serruya, 1974; Hebbert et al., 1979; LaBounty & Horn, 1997; Romero & Imberger, 2003; Effler et al., 2010; Laborde et al., 2010; Cortés et al., 2014) (Fig. S17). During unstratified conditions between late fall and spring, the introduced river water was typically vertically mixed already in RS and ZS before reaching the sill (Fig. S17). Hence, during strong stratification in summer tracer with high concentration was located at comparatively shallow depth in ZS and therefore could be more efficiently transported into GS than during other seasons. In addition, V_{exc} is maximal during summer supporting a larger transport of tracer mass into GS in summer than between fall and spring.

4.2 Impact of climate warming and long-term water level change

Our simulations demonstrate that climate warming and long-term changes in water level can significantly affect the seasonal and the inter-annual pattern of inter-basin exchange in lakes. The change in water exchange patterns is a consequence of changes in ice cover, in thermal stratification, and in water level affecting cross-sectional area and the impact of friction at a sill. In LLC, climate warming leads to reduced ice cover and, at an increase in the air temperature by 4°C, even to ice-free conditions in all years. The model results are consistent with observations from numerous lakes, which have demonstrated a substantial reduction in ice cover with warming over the last century (Magnuson et al., 2000), and with the results from several modeling studies investigating the impact of climate warming on ice cover (Walsh et al., 1998;

Fang & Stefan, 2009; Yao et al., 2014; Woolway & Merchant, 2019; Gronchi et al., 2021). In addition to the loss in ice-cover, our simulations indicate that climate warming results in an earlier onset of stratification, a longer duration of the stratified period and the development of a shallower MLD especially in spring and fall. These predicted changes in stratification are consistent with observations (e.g. Livingstone et al., 2003) and results from several modelling studies (Robertson & Ragotzkie, 1990; Coats et al., 2006; Peeters et al., 2007a, ; MacKay et al., 2009; Perroud et al., 2009; Dibike et al., 2011; Wahl & Peeters, 2014).

The effects of climate warming on ice cover and stratification result in higher inter-basin exchange especially during winter, spring and late fall. These changes in water exchange are caused by changes in the exchange velocity v_s , as is indicated by the large contribution of $\Delta v_{S,m} \cdot A_{S,m,r}$ to $\Delta V_{exc,m}$ (Fig. 9b) whereby $A_{S,m,r}$ refers to $A_{S,m}$ in the same month in scenario T0. The most significant increase in inter-basin exchange occurs during the winter months because the loss of ice cover allows for increased transfer of wind energy to the horizontal currents, i.e. an increased importance of wind driven currents for inter-basin water exchange. The change in stratification apparently also results in larger v_s and thus in larger water exchange, only in spring and late fall, but not during the summer months. During the summer, MLD was already rather small under reference conditions such that climate warming had comparatively small impact on water column stratification and current speed.

In contrast to climate warming an increase in water level (scenario W+) causes the largest increase in water exchange during summer and the smallest in February. The water level increase is associated by an almost proportional increase in the area of the cross-section above the sill, and thus a seasonally homogenous increase in water exchange. However, the contribution due to the increased $A_{S,m}$, to the changes in water exchange caused by scenario W+, $\Delta V_{exc,m}$ ($\Delta V_{exc,m} =$

$\Delta v_{S,m} \cdot A_{S,m,r} + v_{S,m,r} \cdot \Delta A_{S,m} + \Delta v_{S,m} \cdot \Delta A_{S,m}$), increases seasonally (Fig. 9c). Subscript r refers to conditions in the same month in scenario T0. In summer the same change in cross section caused by the water level scenario $\Delta A_{S,m}$ results in a larger contribution $v_{S,m,r} \cdot \Delta A_{S,m}$ than in winter because $v_{S,m,r}$ ($v_{S,m}$ in reference scenario T0) is larger in summer is larger than in winter. In scenario W+, $\Delta v_{S,m}$ contributed as much to $\Delta V_{exc,m}$ as $\Delta A_{S,m}$, and the increase of $v_{S,m}$ was larger in summer than in winter (Fig. 6b). Increased water levels result in larger exchange velocity $v_{S,m}$, because at a higher water level the effects of bottom friction are reduced. Further, at higher water levels the integration in the calculation of $v_{S,m}$ includes velocities at larger distance from the bottom, that typically have a larger magnitude of the component across the transect than currents closer to the sill.

In the scenario with reduced water level (scenario W-) $\Delta v_{S,m} \cdot A_{S,m,r}$ and $v_{S,m,r} \cdot \Delta A_{S,m}$ are both negative because the seasonal changes in $v_{S,m}$ and $A_{S,m}$ are smaller than in the reference scenario T0 (Fig. 9d). Similar to W+, the absolute values of $\Delta v_{S,m} \cdot A_{S,m,r}$ and $v_{S,m,r} \cdot \Delta A_{S,m}$ were about the same and largest in summer (Fig. 9d). Since the absolute change of $v_{S,m}$ caused by W+ with respect to T0 is smaller than the one caused by W-, the absolute value of $\Delta v_{S,m} \cdot A_{S,m,r}$ was larger in W-. This supports the hypothesis that the bottom friction decrease with increasing water level. Climate warming, characterized by an increased air temperature of 4°C, and water level change, characterized by a level increase of 0.3 m throughout the year, have both a strong impact on inter-basin water exchange. The results of the scenarios T4 and W+ show a similar maximum change in V_{exc} but the impact on V_{exc} has an opposite seasonal patterns.

Projections for Lake Constance suggest a reduced seasonal amplitude of water levels, i.e. higher water levels in winter and lower water levels in summer than today (Ostendorp et al., 2020) (scenario $W_{m,w+s-}$, Fig. S15). Consequently, water exchange in scenario $W_{m,w+s-}$ increased

in the winter months and decreased in the summer months. Hence climate warming together with the projected seasonal change in water level will substantially enhance water exchange during the winter months, as increased wind forcing due to reduced ice cover in a warmer climate combines with increased area of the cross-section for water exchange and reduced effects of bottom friction. In summer, in contrast, climate warming has essentially no impact and reduced water levels cause a decrease in V_{exc} . Overall, the seasonal pattern of inter-basin exchange in LLC is therefore expected to change substantially in the future and will be characterized by much stronger water exchange in winter and lower water exchange in summer than today.

However, the seasonal pattern of the water level change in LLC is strongly influenced by the large alpine catchment of ULC with snow melt in the catchment causing a comparatively late increase of the water level in early summer. Projected seasonal water level changes depend on the assumption of a change in precipitation and snow melt during winter. Hence, other lake systems may experience a change in the seasonal pattern of water level due to climate change that differs from that described here in scenario $W_{m,w+s}$. Nevertheless, the results from the scenarios with constant shifts in water level $W+$ and $W-$ provide a good indication of the implications of water level changes and can serve as a guideline for other lakes.

4.3 Implications of the changes in connectivity between basins

The seasonal pattern of water exchange in LLC implies a stronger lateral exchange of dissolved substances and organisms between GS and ZS and thus laterally more homogenous conditions in summer than in winter. In a warmer climate, the increase of water exchange in winter together with the increase in light availability resulting from shorter ice cover duration or absence of ice cover, will impact phytoplankton bloom development in ZS and GS that typically

occurs between January and March (IGKB 2018). Reduced summer water levels predicted for LLC in a warmer climate are expected to cause reduced water exchange and thus larger horizontal differences of dissolved substances and organisms between the sub-basin of LLC especially during summer months. E.g. cyanobacteria typically develop larger abundances in GS than in ZS and RS (IGKB 2012, IGKB 2016). A reduction of the water exchange across the sill in summer may imply a reduction of the export of cyanobacteria from GS to ZS, which may result in larger cyanobacteria populations in GS than today.

Dissolved phosphorus concentrations are typically lower in ULC than in LLC. Thus an increased connectivity between GS and ULC expected for a warmer climate will affect nutrient concentrations in GS especially in winter/early spring and thus may alter primary production during spring bloom and the consecutive plankton development.

Summarizing, climate warming and water level changes not only alter the amount of water exchanged between basins, but also the seasonal pattern of inter basin exchange. The impact of climate warming and water level change on the inter-connectivity between basins therefore can be expected to have a seasonally differential impact on the lateral distribution of dissolved substances and organisms in lakes.

Acknowledgments

This study was financially supported by the German Research Foundation (DFG) within the framework of the RTG R3 (Research Training Group – Responses to biotic and abiotic changes, Resilience and Reversibility of lake ecosystems), grant number 298726046/GRK2272/A4.

We thank Beatrix Rosenberg and Josef Halder, who helped with the field work. We acknowledge Chris Dallimore from Hydronumerics for his help and support with the model setting.

The field datasets (CTD profiles, inflows, outflows and water level) used to set-up the model were provided by the Landesanstalt fuer Umwelt Baden-Wuerttemberg (LUBW), the BOWIS - water information system of Lake Constance from the International Commission for Water Protection of Lake Constance (IGKB), the Hydrographic Service Vorarlberg (VA), and the Swiss Federal Office for the Environment (BAFU). Meteorological data were provided by the German Weather Service (DWD), whereas the COSMO windfield by Meteo Swiss. The model outputs that support these findings are stored in the repository

<https://doi.org/10.5281/zenodo.4472647>.

References

- Aeschbach-Hertig, W., Kipfer, R., Hofer, M., Imboden, D. M., & Baur, H. (1996). Density-driven exchange between the basins of Lake Lucerne (Switzerland) traced with the 3H - 3He method. *Limnology and Oceanography*, *41*(4), 707–721.
- Andersen, M. R., Sand-Jensen, K., Woolway, R. I., & Jones, I. D. (2017). Profound daily vertical stratification and mixing in a small, shallow, wind-exposed lake with submerged macrophytes. *Aquatic Sciences*, *79*(2), 395–406.
- Appt, J., Imberger, J., & Kobus, H. (2004). Basin-scale motion in stratified Upper Lake Constance. *Limnology and Oceanography*, *49*(4), 919–933.
- Bartish, T. (1987). A review of exchange processes among the three basins of Lake Erie. *Journal of Great Lakes Research*, *13*(4), 607–618.
- Beletsky, D., & Schwab, D. J. (2001). Modeling circulation and thermal structure in Lake Michigan: Annual cycle and interannual variability. *Journal of Geophysical Research: Oceans*, *106*(C9), 19745–19771.
- Bennett, J. R. (1974). On the dynamics of wind-driven lake currents. *Journal of Physical Oceanography*, *4*(3), 400–414.
- Caramatti, I., Peeters, F., Hamilton, D., & Hofmann, H. (2020). Modelling inter-annual and spatial variability of ice cover in a temperate lake with complex morphology. *Hydrological Processes*.
- Chen, C. A., & Millero, F. J. (1986). Thermodynamic properties for natural waters covering only the limnological range 1. *Limnology and Oceanography*, *31*(3), 657–662.
- Coats, R., Perez-Losada, J., Schladow, G., Richards, R., & Goldman, C. (2006). The warming of lake Tahoe. *Climatic Change*, *76*(1–2), 121–148.

Cortés, A., Fleenor, W. E., Wells, M. G., de Vicente, I., & Rueda, F. J. (2014). Pathways of river water to the surface layers of stratified reservoirs. *Limnology and Oceanography*, *59*(1), 233–250.

Dissanayake, P., Hofmann, H., & Peeters, F. (2019). Comparison of results from two 3D hydrodynamic models with field data: Internal seiches and horizontal currents. *Inland Waters*, *9*(2), 239–260.

Effler, S. W., Prestigiacomo, A. R., Effler, A. J. P., & Driscoll, C. (2010). Water quality patterns in a river-lake system from multiple drivers (Three Rivers, New York State). *River Systems*, *19*(1), 75–94.

Fang, X., & Stefan, H. G. (2009). Simulations of climate effects on water temperature, dissolved oxygen, and ice and snow covers in lakes of the contiguous US under past and future climate scenarios. *Limnology and Oceanography*, *54*(6part2), 2359–2370.

Fujisaki, A., Wang, J., Bai, X., Leshkevich, G., & Lofgren, B. (2013). Model-simulated interannual variability of Lake Erie ice cover, circulation, and thermal structure in response to atmospheric forcing, 2003–2012. *Journal of Geophysical Research: Oceans*, *118*(9), 4286–4304.

Giling, D. P., Staehr, P. A., Grossart, H. P., Andersen, M. R., Boehrer, B., Escot, C., ... Obrador, B. (2017). Delving deeper: Metabolic processes in the metalimnion of stratified lakes. *Limnology and Oceanography*, *62*(3), 1288–1306. <https://doi.org/10.1002/lno.10504>

Gregg, M. C. (2004). Small-scale processes in straits. *Deep Sea Research Part II: Topical Studies in Oceanography*, *51*(4–5), 489–503.

Haghighi, A. T., & Kløve, B. (2015). A sensitivity analysis of lake water level response to changes in climate and river regimes. *Limnologica*, *51*, 118–130.

Hebbert, B., Patterson, J., Loh, I., & Imberger, J. (1979). Collie river underflow into the Wellington reservoir. *Journal of Hydraulic Engineering*, 105(5), 533–545.

Hodges, B. R. (2000). Numerical Techniques in CWR-ELCOM (code release v. 1). *CWR Manuscript WP*, 1422.

Hodges, B. R., Imberger, J., Saggio, A., & Winters, K. B. (2000). Modeling basin-scale internal waves in a stratified lake. *Limnology and Oceanography*, 45(7), 1603–1620.

Hodges, B. (1998). Heat budget and thermodynamics at a free surface: Some theory and numerical implementation. *Centre for Water Research, University of Western Australia, Crawley, WA, Australia*.

Hodges, Ben, & Dallimore, C. (2018). *HydroNumerics*.

Hohmann, R., Hofer, M., Kipfer, R., Peeters, F., Imboden, D. M., Baur, H., & Shimaraev, M. N. (1998). Distribution of helium and tritium in Lake Baikal. *Journal of Geophysical Research: Oceans*, 103(C6), 12823–12838.

Igkb. (2012). Limnologischer Zustand des Bodensees. *Grüner Bericht Nr. 40*, (39).

Igkb. (2016). Limnologischer Zustand des Bodensees. *Grüner Bericht Nr. 40*, (41).

Igkb. (2018). Limnologischer Zustand des Bodensees. *Grüner Bericht Nr. 40*, (42).

Kupisch, M., Moenickes, S., Schlieff, J., Frassl, M., & Richter, O. (2012). Temperature-dependent consumer-resource dynamics: A coupled structured model for *Gammarus pulex* (L.) and leaf litter. *Ecological Modelling*, 247, 157–167.

Laborde, S., Antenucci, J. P., Copetti, D., & Imberger, J. (2010). Inflow intrusions at multiple scales in a large temperate lake. *Limnology and Oceanography*, 55(3), 1301–1312.

LaBounty, J. F., & Horn, M. J. (1997). The influence of drainage from the Las Vegas valley on the limnology of Boulder Basin, Lake Mead, Arizona-Nevada. *Lake and Reservoir Management*, 13(2), 95–108.

Laval, B., Imberger, J., Hodges, B. R., & Stocker, R. (2003). Modeling circulation in lakes: Spatial and temporal variations. *Limnology and Oceanography*, 48(3), 983–994.

Liu, S., Ye, Q., Wu, S., & Stive, M. J. F. (2018). Horizontal circulation patterns in a large shallow lake: Taihu Lake, China. *Water*, 10(6), 792.

Livingstone, D. M. (2003). Impact of secular climate change on the thermal structure of a large temperate central European lake. *Climatic Change*, 57(1–2), 205–225.

Luft, G., & van den Eertwegh, G. (1991). Long-term changes in the water level of Lake Constance and possible causes. *Proc. Vienna Symp. Hydrology of Natural and Manmade Lakes. IAHS Publ. 206*, 31–44.

MacIntyre, S., Romero, J. R., & Kling, G. W. (2002). Spatial-temporal variability in surface layer deepening and lateral advection in an embayment of Lake Victoria, East Africa. *Limnology and Oceanography*, 47(3), 656–671.

Magnuson, J. J., Robertson, D. M., Benson, B. J., Wynne, R. H., Livingstone, D. M., Arai, T., ... Kuusisto, E. (2000). Historical trends in lake and river ice cover in the Northern Hemisphere. *Science*, 289(5485), 1743–1746.

Michel, A., Brauchli, T., Lehning, M., Schaefli, B., & Huwald, H. (2020). Stream temperature and discharge evolution in Switzerland over the last 50 years: annual and seasonal behaviour. *Hydrology and Earth System Sciences*, 24(1), 115–142.

Mishra, V., Cherkauer, K. A., Bowling, L. C., & Huber, M. (2011). Lake Ice phenology of small lakes: Impacts of climate variability in the Great Lakes region. *Global and Planetary Change*, 76(3–4), 166–185.

Nguyen, T. D., Hawley, N., & Phanikumar, M. S. (2017). Ice cover, winter circulation, and exchange in Saginaw Bay and Lake Huron. *Limnology and Oceanography*, 62(1), 376–393.

Nguyen, T. D., Thupaki, P., Anderson, E. J., & Phanikumar, M. S. (2014). Summer circulation and exchange in the Saginaw Bay-Lake Huron system. *Journal of Geophysical Research: Oceans*, 119(4), 2713–2734.

Niu, Q., Xia, M., Rutherford, E. S., Mason, D. M., Anderson, E. J., & Schwab, D. J. (2015). Investigation of interbasin exchange and interannual variability in Lake Erie using an unstructured-grid hydrodynamic model. *Journal of Geophysical Research: Oceans*, 120(3), 2212–2232.

O'Reilly, C. M., Sharma, S., Gray, D. K., Hampton, S. E., Read, J. S., Rowley, R. J., ... Kraemer, B. M. (2015). Rapid and highly variable warming of lake surface waters around the globe. *Geophysical Research Letters*, 42(24), 10–773.

Oveisy, A., Boegman, L., & Imberger, J. (2012). *Three-dimensional simulation of lake and ice dynamics during winter*. 57(1), 43–57. <https://doi.org/10.4319/lo.2012.57.1.0043>

Peeters, F. (2000). Correction to “Vertical turbulent diffusion and upwelling in Lake Baikal estimated by inverse modeling of transient tracers” by F. Peeters, R. Kipfer, M. Hofer, DM Imboden, and VM Domysheva. *J. Geophys. Res*, 105(14,283).

Peeters, F., Straile, D., Lorke, A., & Livingstone, D. M. (2007a). Earlier onset of the spring phytoplankton bloom in lakes of the temperate zone in a warmer climate. *Global Change Biology*, 13(9), 1898–1909.

Peeters, F., Straile, D., Lorke, A., & Ollinger, D. (2007b). Turbulent mixing and phytoplankton spring bloom development in a deep lake. *Limnology and Oceanography*, 52(1), 286–298.

Rao, Y. R., Marvin, C. H., & Zhao, J. (2009). Application of a numerical model for circulation, temperature and pollutant distribution in Hamilton Harbour. *Journal of Great Lakes Research*, 35(1), 61–73.

Razmi, A. M., Barry, D. A., Lemmin, U., Bonvin, F., Kohn, T., & Bakhtyar, R. (2014). Direct effects of dominant winds on residence and travel times in the wide and open lacustrine embayment: Vidy Bay (Lake Geneva, Switzerland). *Aquatic Sciences*, 76(1), 59–71.

Read, J. S., Hamilton, D. P., Jones, I. D., Muraoka, K., Winslow, L. A., Kroiss, R., ... Gaiser, E. (2011). Derivation of lake mixing and stratification indices from high-resolution lake buoy data. *Environmental Modelling and Software*, 26(11), 1325–1336.

<https://doi.org/10.1016/j.envsoft.2011.05.006>

Robertson, D. M., & Ragotzkie, R. A. (1990). Changes in the thermal structure of moderate to large sized lakes in response to changes in air temperature. *Aquatic Sciences*, 52(4), 360–380.

Romero, J. R., & Imberger, J. (2003). Effect of a flood underflow on reservoir water quality: Data and three-dimensional modeling. *Archiv Für Hydrobiologie*, 157(1), 1–25.

Rueda, F. J., & Cowen, E. A. (2005). Exchange between a freshwater embayment and a large lake through a long, shallow channel. *Limnology and Oceanography*, 50(1), 169–183.

Schlatter, J. W., Wüest, A., & Imboden, D. M. (1997). Hypolimnetic density currents traced by sulphur hexafluoride (SF₆). *Aquatic Sciences*, 59(3), 225–242.

Serruya, S. (1974). The mixing patterns of the Jordan River in Lake Kinneret 1. *Limnology and Oceanography*, 19(2), 175–181.

Straile, D., Kerimoglu, O., & Peeters, F. (2015). Trophic mismatch requires seasonal heterogeneity of warming. *Ecology*, 96(10), 2794–2805.

Trolle, D., Hamilton, D. P., Pilditch, C. A., Duggan, I. C., & Jeppesen, E. (2011). Predicting the effects of climate change on trophic status of three morphologically varying lakes: Implications for lake restoration and management. *Environmental Modelling & Software*, 26(4), 354–370.

Umlauf, L., & Lemmin, U. (2005). Interbasin exchange and mixing in the hypolimnion of a large lake: The role of long internal waves. *Limnology and Oceanography*, 50(5), 1601–1611.

Wahl, B., & Peeters, F. (2014). Effect of climatic changes on stratification and deep-water renewal in Lake Constance assessed by sensitivity studies with a 3D hydrodynamic model. *Limnology and Oceanography*, 59(3), 1035–1052.

Walsh, S. E., Vavrus, S. J., Foley, J. A., Fisher, V. A., Wynne, R. H., & Lenters, J. D. (1998). Global patterns of lake ice phenology and climate: Model simulations and observations. *Journal of Geophysical Research: Atmospheres*, 103(D22), 28825–28837.

Weiss, R. F., Carmack, E. C. C., & Koropalov, V. M. (1991). Deep-water renewal and biological production in Lake Baikal. *Nature*, 349(6311), 665–669.

Woodward, B. L., Marti, C. L., Imberger, J., Hipsey, M. R., & Oldham, C. E. (2017). Wind and buoyancy driven horizontal exchange in shallow embayments of a tropical reservoir: Lake Argyle, Western Australia. *Limnology and Oceanography*, 62(4), 1636–1657.

Woolway, R. I., & Merchant, C. J. (2019). Worldwide alteration of lake mixing regimes in response to climate change. *Nature Geoscience*, *12*(4), 271–276.

Yao, H., Samal, N. R., Joehnk, K. D., Fang, X., Bruce, L. C., Pierson, D. C., ... James, A. (2014). Comparing ice and temperature simulations by four dynamic lake models in Harp Lake: past performance and future predictions. *Hydrological Processes*, *28*(16), 4587–4601.

Effects of climate change on inter-basin exchange in Lower Lake Constance

I. Caramatti¹, H. Hofmann¹ and F. Peeteers¹

¹ University of Konstanz, Konstanz, Germany

Contents of this file

Text S1 to S9
Figures S1 to S22
Tables S1 to Sx6

Introduction

The Supporting Information includes text, figures and tables that illustrates:

- the set-up of the coarse model of LC (Text S1) and the derived water temperature of the river Seerhein (Fig. S1)
- the model validation in LLC (Text S2-S3, Fig. S2 – S3, Tab. S1)
- the simulated lake thermal structure in GS and ZS (Fig. S4 – S7, Tab. S2 – S3)
- the grid of the COSMO windfield and the seasonal pattern of wind at the sill (Text S4, Fig. S8 – S9)
- the statistical analysis used to investigate potential links between parameters (Text S5 – S7, Tab. S4 – S6)
- the comparison of currents at the sill and at the station M_{GS} and M_{ZS} (Text S8, Fig. S10 – S12)
- the results of the sensitivity analysis (Text S9, Fig. S13)
- the maximum ice coverage of the lake surface in the scenarios (T0, W+ and W-) (Fig. S14)
- the seasonal water level scenarios and the results in the reference scenario W_m (Fig. S15-S16)
- the results of the tracer experiments (Fig. S17 – S22)

Text S1.

The hydrodynamic model of LC used to derive the inflow temperature of the Seerhein was previously set up and validated in Caramatti et al. (2019). The model was characterized by a 300 m x 300 m horizontal grid and 70 vertical layers of variable thickness. The vertical resolution was 1 m in the upper 29 layers and 10 m in the lower 10 layers. Between the 30th and 57th layer the vertical resolution varied slowly between 1 and 10 m. The major inflows of LC, according to Stewart (1988), were considered and the water level was kept constant to the mean water level during the simulated period (396 m.a. s. l.), by adjusting the outflow discharge with a water balance.

Water temperature in LC was initialized by means of data from a thermistor chain (RBR-solo, vertical resolution 0.5 to 2 m in the upper 20 m and coarser below) at the station EU, the deepest station in the Überlingen basin of ULC, and data with a coarser resolution (from 5 to 20 m) from the Landesanstalt fuer Umwelt Baden-Wuerttemberg (LUBW) at station FU (the deepest point of ULC), M_{GS} , M_{ZS} and M_{RH} . Horizontally resolved wind fields (COSMO-MeteoSwiss, resolution 2.2 km until August 2016 and then 1.1 km) were linearly interpolated to the computational grid of LC. Except for the wind field, the model was driven with horizontally uniform meteorological data. For the climate warming scenario (T4) the model was run with increased air temperature (+4°C) and increased inflow temperature (95% of the increase in air temperature). The new initial conditions were derived after a pre-run repeating the meteorological and flow conditions of the year 2009 in a warmer scenario.

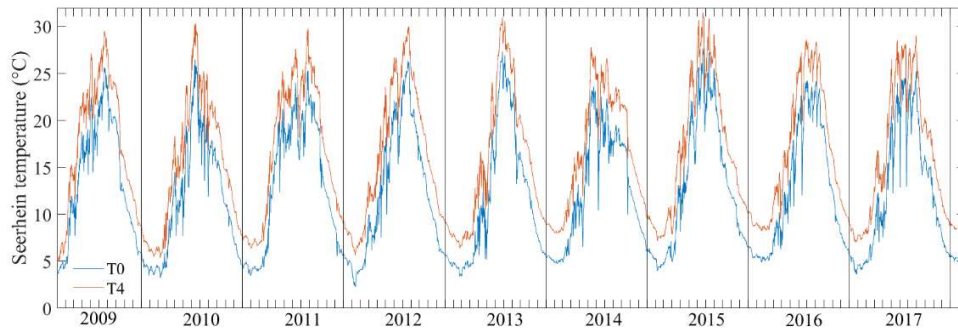


Figure S1. Simulated multi-annual course of Seerhein temperature in the scenarios T0 and T4.

Text S2.

Model results and observations of water temperature were compared at the two stations M_{GS} and M_{ZS} for three consecutive years (2010, 2011, and 2012) to validate the model performance in terms of thermal structure throughout the season and among years (Fig. S2).

The agreement between simulated thermal structure and monthly temperature profiles was evaluated using the root mean square error (RMSE). A mean RMSE was computed for each of the four periods described above (December-March, April-May, June-September, October-November) and is presented in Tab. S1. The model represents the thermal structure most accurately between October and March, with a mean RMSE between 0.37 and 1.08°C in ZS and 0.97 and 1.82°C in GS. During the winter months (from December-March), the mean RMSE was 0.85, 0.37, 0.45°C in ZS for the years 2010, 2011, 2012 and 1.03, 0.98°C in GS for the years 2010, 2012 (no data available in 2011). The simulation was least accurate in the period June-September, with a maximum mean RMSE of 1.49 at MZS and 2.34°C at M_{GS} . In each case, the model reproduced the thermal structure more accurately at station M_{ZS} than at M_{GS} . Text published in caramatti et al. (2020).

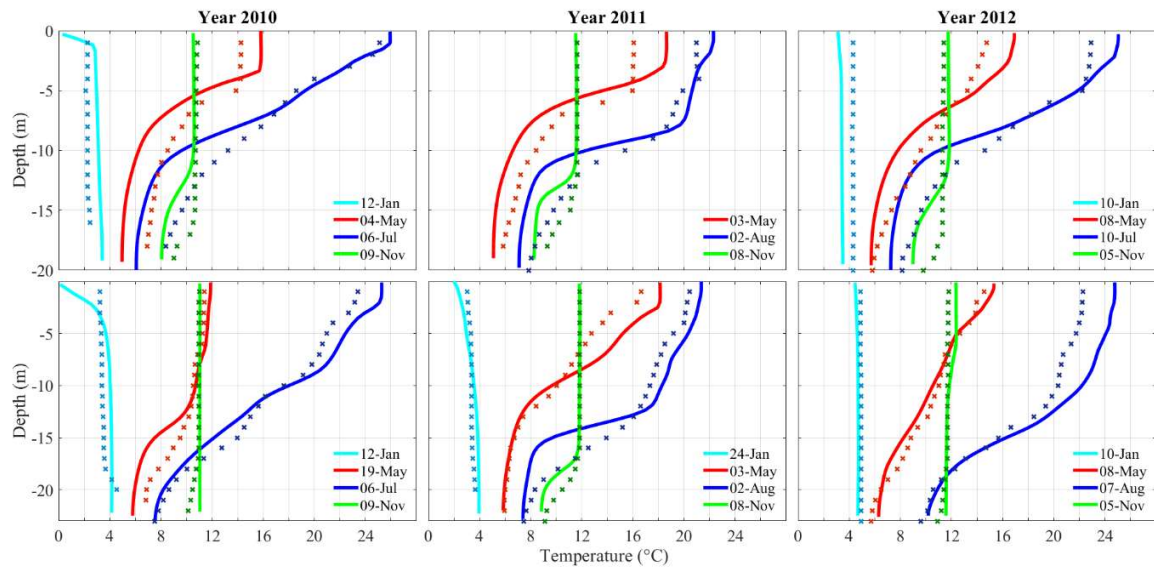


Figure S2. Model validation: Seasonal differences in thermal structure between observed (continuous line) and simulated (dotted line) temperature in Gnadensee (GS) and Zeller See (ZS) for characteristic snapshots of three consecutive years (2010, 2011 and 2012). Figure published in Caramatti et al. (2020).

Gnadensee				
RMSE (°C)	Dec. - March	April - May	June – Sept.	Oct. – Nov.
2010	1.03	2.16	2.26	1.03
2011	-	2.01	2.06	1.82
2012	0.98	1.59	2.34	0.97
Zeller See				
RMSE (°C)	Dec. - March	April - May	June – Sept.	Oct. – Nov.
2010	0.85	1.12	1.32	1.02
2011	0.37	0.97	2.22	1.08
2012	0.45	0.51	1.49	0.35

Table S1. Model validation based on temperature. RMSE between measured and simulated temperature profiles of the sub-basins Gnadensee and Zeller See. Table published in Caramatti et al. (2020).

Text S3.

The simulated current velocities across the sill between Gnadensee (GS) and Zeller See (ZS) were compared with field measurements taken with an Aquadopp HR Profiler (Nortek) at position M_{AQ} (Fig. S3). The field instrument was looking upward measuring between 0.7 – 1.7 m above the ground (mean water depth: 2.5 m) with a high vertical resolution of 0.05 m and a sampling rate of 5 s. Field data was collected between 7/7/2018 – 28/11/2018. The model output was extrapolated at the position M_{AQ} and at the depth investigated by the Aquadopp. The simulated components of the current velocity were interpolated to the time of the field measurements (1 hour interval). Both time series were then smoothed weekly and thereafter the RMSE between model and data was calculated.

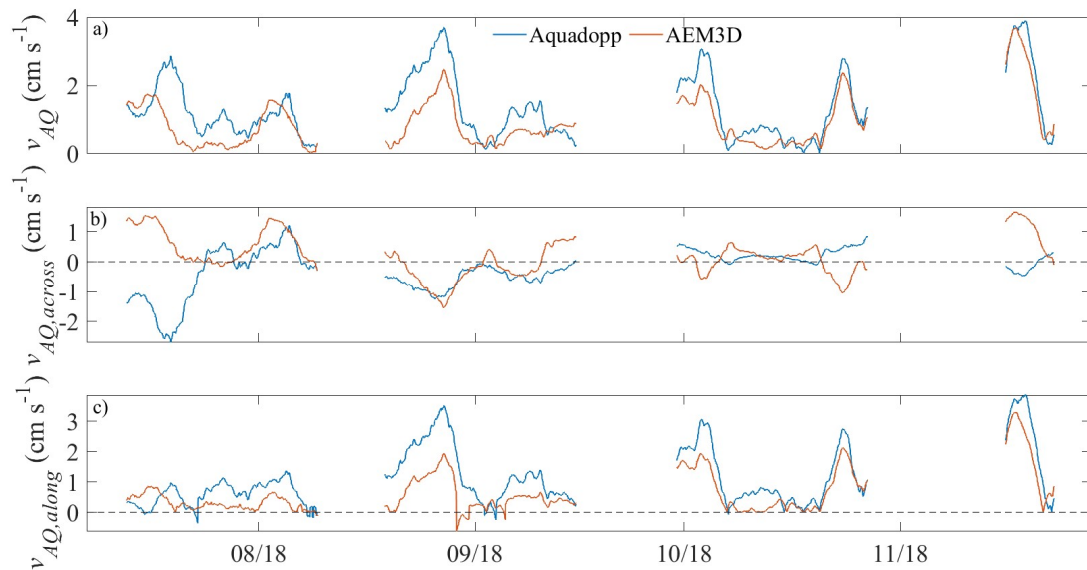


Figure S3. Model validation of currents across the sill between GS and ZS. Comparison between observed (blue) and simulated (orange) current speed (v_{AQ}), as well as the along- and across-velocity components ($v_{AQ,along}$ and $v_{AQ,across}$) at station M_{AQ} with respect to $Trans_{M-R}$.

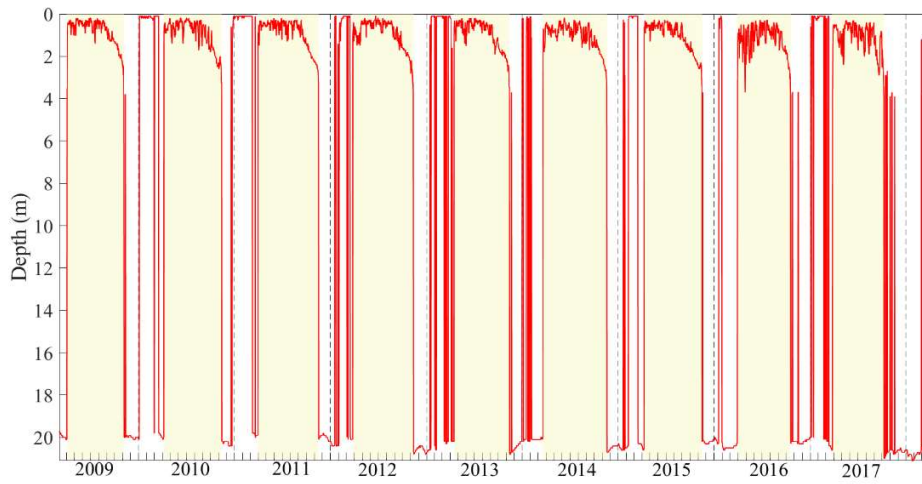


Figure S4. Simulated MLD_{GS} . The duration of the stratification period at M_{GS} is shaded in yellow.

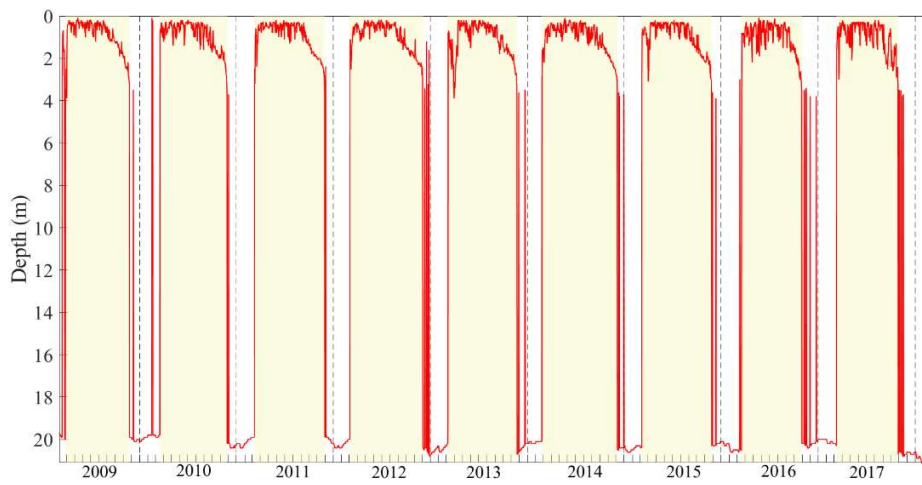


Figure S5. Simulated MLD_{GS} in the scenario T4. The duration of the stratification period at M_{GS} is shaded in yellow.

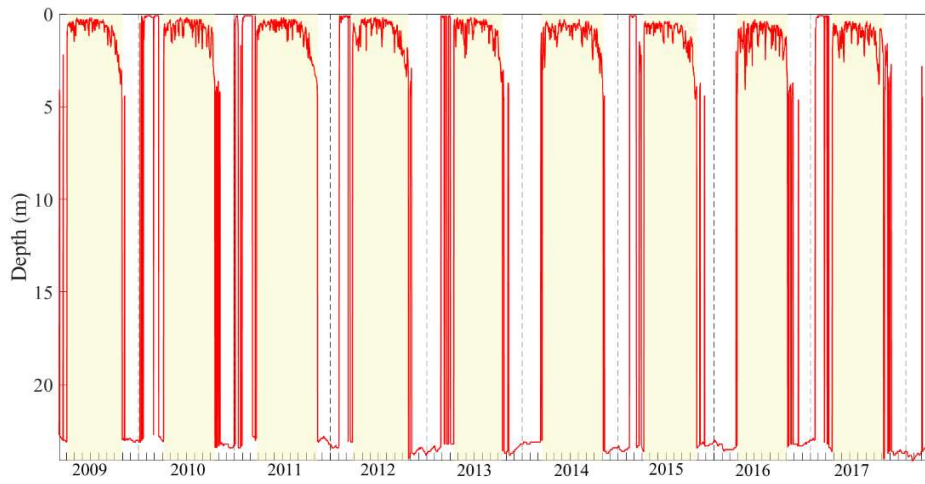


Figure S6. Simulated MLD_{ZS} . The duration of the stratification period at M_{ZS} is shaded in yellow.

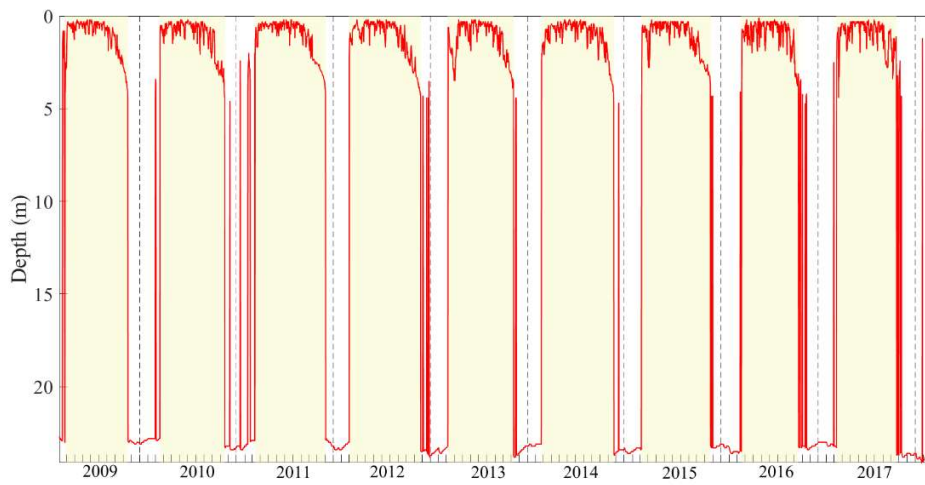


Figure S7. Simulated MLD_{ZS} in the scenario T4. The duration of the stratification period at M_{ZS} is shaded in yellow.

Year	Beginning of stratification (doy)	Ending of stratification (doy)	Duration stratification (days)	Δ Beginning of stratification (days)	Δ Ending of stratification (days)	Δ Duration of stratification (days)
Scenario T0						
2009	91	308	217	-	-	-
2010	95	315	220	-	-	-
2011	88	319	231	-	-	-
2012	84	315	231	-	-	-
2013	104	315	211	-	-	-
2014	77	321	244	-	-	-
2015	98	318	220	-	-	-
2016	88	291	203	-	-	-
2017	84	280	196	-	-	-
Average	90	309	219	-	-	-
Scenario T4						
2009	85	326	241	- 6	18	24
2010	76	329	253	- 19	14	33
2011	69	333	264	- 19	14	33
2012	61	336	275	- 23	21	44
2013	90	325	235	- 14	10	24
2014	53	339	286	- 24	18	42
2015	65	329	264	- 33	11	44
2016	76	304	228	- 12	13	25
2017	68	300	232	- 16	20	36
Average	71	325	253	- 18	15	34

Table S2. Timing and deviation of the summer stratification period between the reference scenario T0 and the climate change scenario T4 at station M_{GS}.

Year	Beginning of stratification (doy)	Ending of stratification (doy)	Duration stratification (days)	Δ Beginning of stratification (days)	Δ Ending of stratification (days)	Δ Duration of stratification (days)
Scenario T0						
2009	91	301	210	-	-	-
2010	94	289	195	-	-	-
2011	83	315	232	-	-	-
2012	83	296	213	-	-	-
2013	103	288	185	-	-	-
2014	75	307	232	-	-	-
2015	97	298	201	-	-	-
2016	87	279	192	-	-	-
2017	83	278	195	-	-	-
Average	88	295	206	-	-	-
Scenario T4						
2009	83	320	237	- 8	19	27
2010	76	320	244	- 18	31	49
2011	69	335	266	- 14	20	34
2012	59	328	269	- 24	32	56
2013	65	312	247	- 38	24	62
2014	52	325	273	- 23	18	41
2015	64	324	260	- 33	26	59
2016	76	291	215	- 11	12	23
2017	68	294	226	- 15	16	31
Average	68	317	249	- 20	22	42

Table S3. Timing and deviation of the summer stratification period between the reference scenario T0 and the climate change scenario T4 at station M_{ZS}.

Text S4.

The COSMO wind field (MeteoSwiss) was linearly interpolated to the computational grid of LLC and ULC. The wind field had a spatial resolution of 2.2 km before August 2016 and afterwards 1.1 km. The north- and east-wind components were derived in the closest points to $\text{Trans}_{\text{M-R}}$ of both grids (Fig. S8) to investigate their correlation with the inter-basin water exchange.

Wind components were computed along and across $\text{Trans}_{\text{M-R}}$ ($Across_w$, $Along_w$) and then averaged monthly to observe the existence of a wind seasonal pattern. The wind speed, WS , and direction, WD , were computed from the monthly-averaged north- and east-wind components.

The wind flows on average south-westwards (from GS to ZS). However, the average speed of the wind flow across and along the sill did not show a pronounced seasonal pattern (Fig. S9).

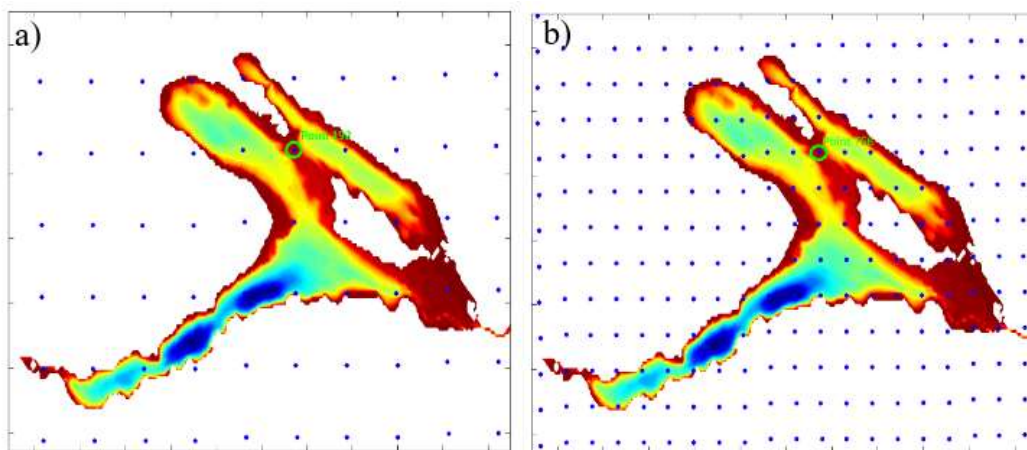


Figure S8. Selected points closest to $\text{Trans}_{\text{M-R}}$ of the wind field a) with a 2.2 km (station 192) and b) 1.1 km) resolution (station 766).

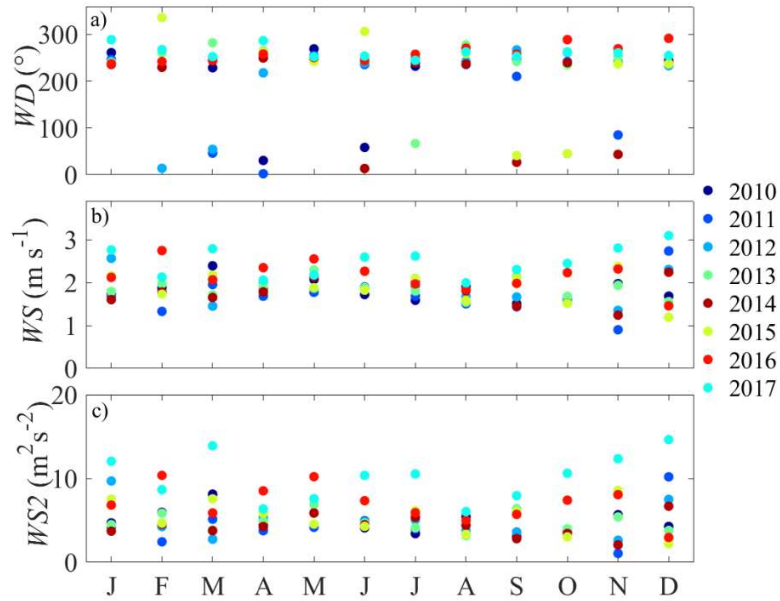


Figure S9. Seasonal pattern of monthly-averaged wind at the grid point of the COSMO windfield closest to $\text{Trans}_{\text{M-R}}$ (station 192 and 766). Note that the wind direction WD is expressed relative to the north direction and $WS2$ represents the wind speed squared, which is proportional to the wind forcing at the lake surface.

Text S5.

Linear regression analysis was applied to investigate potential links between V_{exc} , WL_S , A_S , v_s , MLD_{SI} , WS (Fig. 4). The analysis was performed using multi-annual averages (January 2010 to December 2017) of monthly-mean data from considering two different data sets: a) considering the ice free season April to December and (b) considering all month.

		r	R^2	p -value
$WL_{S,m}$	$V_{exc,m}$	0.93	0.86	<0.001
$A_{S,m}$	$V_{exc,m}$	0.93	0.86	<0.001
$v_{S,m}$	$V_{exc,m}$	0.99	0.98	<0.001
$MLD_{SI,m}$	$V_{exc,m}$	-0.83	0.69	0.01
$WL_{S,m}$	$v_{S,m}$	0.87	0.77	<0.001
$MLD_{SI,m}$	$v_{S,m}$	-0.82	0.68	0.01
$WL_{S,m}$	$A_{S,m}$	-0.77	0.60	0.01
$MLD_{SI,m}$	$WL_{S,m}$	-0.77	0.60	0.01
$MLD_{SI,m}$	$A_{S,m}$	1.00	1.00	<0.001
WS_m	$V_{exc,m}$	0.24	0.06	0.54
WS_m	$v_{S,m}$	0.32	0.10	0.40

Table S4. Results from the regression analyses of the seasonal change in multi-annual averages of monthly mean values considering the ice free season April to December. The variables included in this analysis are the multi-annual averages (years 2010-2017) of monthly-mean properties water exchange $V_{exc,m}$, water level $WL_{S,m}$, area of the cross-section above along Trans_{M-R} the sill $A_{S,m}$, current speed across Trans_S, $v_{S,m}$, mixed layer depth at the station M_{SI} $MLD_{SI,m}$, and wind speed close to the sill WS_m .

		r	R^2	p -value
$WL_{S,m}$	$V_{exc,m}$	0.95	0.91	<0.001
$A_{S,m}$	$V_{exc,m}$	0.95	0.91	<0.001
$v_{S,m}$	$V_{exc,m}$	0.99	0.98	<0.001
$MLD_{Sl,m}$	$V_{exc,m}$	-0.56	0.31	0.06
$WL_{S,m}$	$v_{S,m}$	0.92	0.84	<0.001
$MLD_{Sl,m}$	$v_{S,m}$	-0.50	0.25	0.10
$WL_{S,m}$	$A_{S,m}$	-0.52	0.27	0.08
$MLD_{Sl,m}$	$WL_{S,m}$	-0.52	0.27	0.08
$MLD_{Sl,m}$	$A_{S,m}$	1.00	1.00	<0.001
WS_m	$V_{exc,m}$	0.00	0.00	0.99
WS_m	$v_{S,m}$	0.04	0.00	0.89

Table S5. Results from the regression analyses of the seasonal change in multi-annual averages of monthly mean values considering all months. The variables included in this analysis are the multi-annual averages (years 2010-2017) of monthly-mean properties water exchange $V_{exc,m}$, water level $WL_{S,m}$, area of the cross-section above along $Trans_{M-R}$ the sill $A_{S,m}$, current speed across $Trans_S$, $v_{S,m}$, mixed layer depth at the station M_{Sl} $MLD_{Sl,m}$, and wind speed close to the sill WS_m .

Text S6.

Linear regression analysis was applied to investigate potential links between V_{exc} and v_s above and below the MLD_s and other properties relevant for water exchange at the sill (WL_s , A_s , MLD_s , WS). The analysis was performed using multi-annual averages (January 2010 to December 2017) of monthly-mean data considering the ice free season April to December.

		r	R^2	p -value
$WL_{S,m}$	$V_{exc,ML,m}$	0.17	0.03	0.67
$MLD_{SI,m}$	$V_{exc,ML,m}$	0.28	0.08	0.47
$WL_{S,m}$	$V_{exc,B,m}$	0.92	0.85	<0.001
$MLD_{SI,m}$	$V_{exc,B,m}$	-0.92	0.84	<0.001
$WL_{S,m}$	$v_{S,ML,m}$	0.88	0.77	<0.001
$MLD_{SI,m}$	$v_{S,ML,m}$	-0.87	0.76	<0.001
$WL_{S,m}$	$v_{S,B,m}$	0.90	0.81	<0.001
$MLD_{SI,m}$	$v_{S,B,m}$	-0.92	0.84	<0.001

Table S6. Linear regression analysis of the seasonal change V_{exc} and v_S above and below the mixed layer depth along $Trans_{M-R}$, MLD_S , as function of water level and mixed layer depth at M_{SI} , MLD_{SI} . Analyses are based on multi-annual average monthly-mean data and consider only the ice-free season from April to December.

Text S7.

Climate warming induced changes in monthly mean current speed across the sill (Δv_S , $\Delta v_{S,ML}$, $\Delta v_{S,B}$) and in water exchange (ΔV_{exc} , $\Delta V_{exc,ML}$, $\Delta V_{exc,B}$) were compared to changes in monthly MLD at the station M_{SI} (ΔMLD_{SI}) using linear regression analysis (Tab. S6). The change of a property indicated by Δ is the monthly mean difference between the value of this property in scenario T4 minus its value in scenario T0. The regression analyses only consider the ice-free season from April to December.

		r	R^2	p -value
ΔMLD_{SI}	ΔV_{exc}	-0.46	0.21	0.21
ΔMLD_{SI}	$\Delta V_{exc,ML}$	0.59	0.35	0.09
ΔMLD_{SI}	$\Delta V_{exc,B}$	-0.82	0.67	0.01
ΔMLD_{SI}	Δv_S	-0.51	0.26	0.16
ΔMLD_{SI}	$\Delta v_{S,ML}$	-0.60	0.36	0.09
ΔMLD_{SI}	$\Delta v_{S,B}$	-0.87	0.76	<.0001

Table S6. Results on from a linear regression analysis comparing the impact of climate warming on water exchange and on exchange velocity with the corresponding change in mixed layer depth at the deepest station on the sill (ΔMLD_{SI}). Analyses are based on monthly-mean data. Δ indicates the difference between the monthly mean value in scenario T4 minus its value in scenario T0. The linear regression considered only the ice-free season from April to December

Text S8.

The vertical and seasonal pattern of the simulated currents at the sill were compared with the simulated currents at the stations M_{GS} and M_{ZS} . The vertical profiles of current speed in M_{GS} , M_{ZS} and M_{SI} , and the across speed component at M_{SI} were averaged monthly and between the years 2010 - 2017. The profiles were then compared in the months July and December, as representative of stratified and fully-mixed water column (Fig. S10a-d).

Additionally, we vertically averaged the monthly-mean current speeds at M_{GS} , M_{ZS} and M_{SI} , and the across speed component at M_{SI} to compare the seasonal pattern in the open water of Gnadensee and Zellersee and at the deepest station on the sill. The currents speeds were averaged from the water surface to the maximum water depth at the deepest station of the sill.

The vertical current velocity components at M_{GS} and M_{ZS} were compared in three different periods of the year 2010, as representative of the different thermal conditions in the lake: in April (establishment of stratification), in July (stable stratification) and in November (fully-mixed water column). For each month, 10 days were shown in the figures S11 and S12.

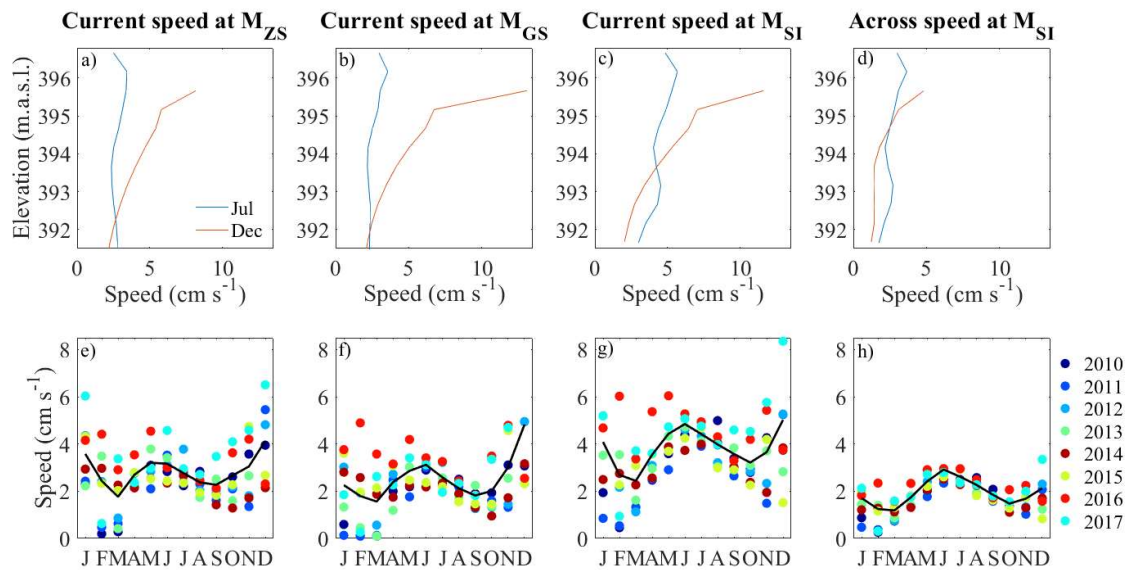


Figure S10. Vertical profiles and seasonal changes of mean currents in the open water of Gnadensee and Zellersee and at the deepest station of the sill. Profiles are multi-annual averages (2010-2017) of monthly mean current profiles for July and December at station a) M_{GS} , b) M_{ZS} and c) M_{SI} . In addition, similarly constructed profiles of the speed of the current across the sill at the deepest station of the sill are depicted in d). The symbols in e-h show the monthly mean vertically averaged current speed at e) M_{GS} , f) M_{ZS} and g) M_{SI} and h) of the speed across the sill at M_{SI} . The vertical profiles and the vertical averages extend over the elevation range from the deepest point of the sill to the water surface. The multi-annual averages consider only the depth range available in all years, i.e. from the surface down to the multi-annual minimum of the monthly mean D_s . The black line connects the multi-annual average of the monthly values (years 2010 – 2017).

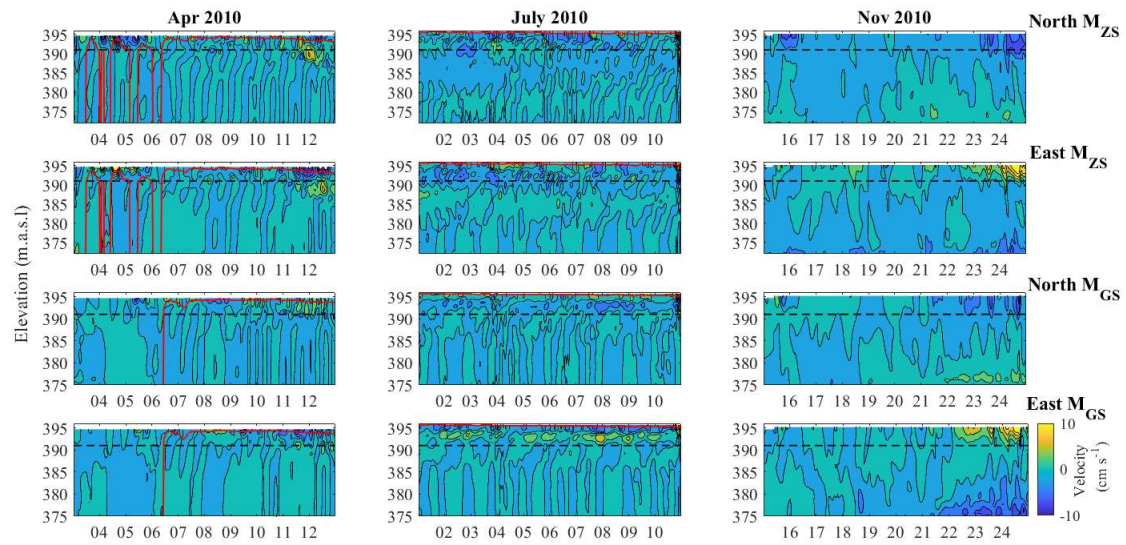


Figure S11. Currents in M_{GS} and M_{ZS}. The north and east components of the current velocity at M_{GS} and M_{ZS} were compared for the year 2010 in April (establishment of stratification), in July (stable stratification) and in November (fully-mixed water column). The mixed layer depth at M_{GS} and M_{ZS} is indicated by a red line, whereas the dashed line refers to the minimum elevation of Trans_{M-R}.

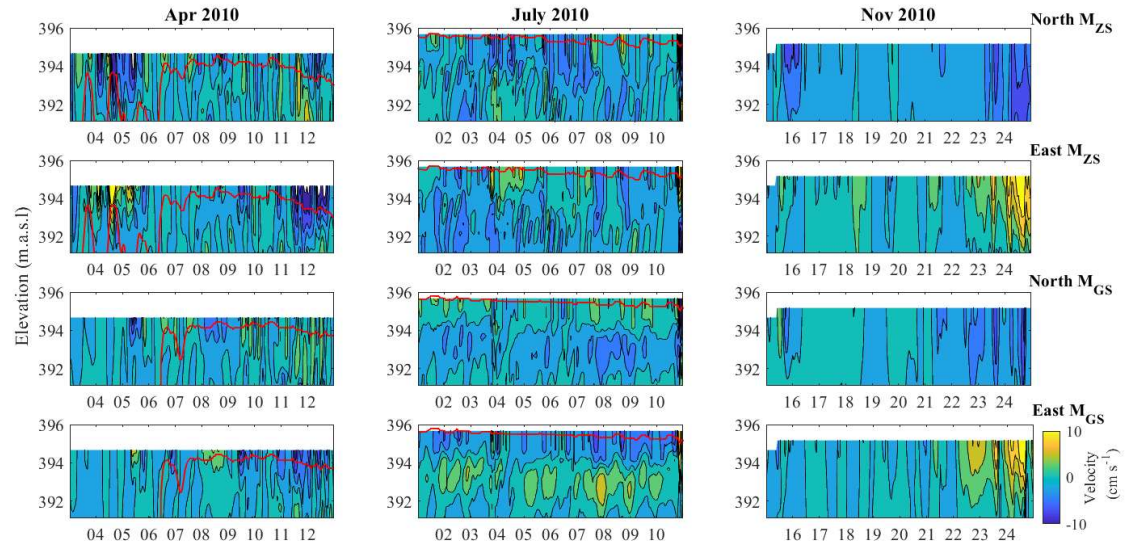


Figure S12. Currents at M_{GS} and M_{ZS} from the surface down to the minimum elevation of $Trans_{M-R}$. The north and east components of the current velocity at M_{GS} and M_{ZS} were compared for the year 2010 in April (establishment of stratification), in July (stable stratification) and in November (fully-mixed water column). The mixed layer depth at M_{GS} and M_{ZS} is indicated by a red line.

Text S9.

A sensitivity analysis was conducted to investigate the seasonal change of V_{exc} and v_s to relative to the seasonal change in water level by applying a scenario in which the outflow was adjusted to provide a constant water level in LLC with all other conditions being the same as in scenario T0. The year 2010 was used as reference for the analysis. The scenario considered a constant water level from April to December (IO_A).

The response of the system to the scenarios was analyzed at the sill comparing the monthly-mean water exchange (V_{exc}) and mean current speed (v_s) with the reference scenario T0, and at the stations M_{GS} and M_{ZS} comparing the monthly- and vertically-averaged current speed (v_{GZ} and v_{ZS}) of IO_A with T0.

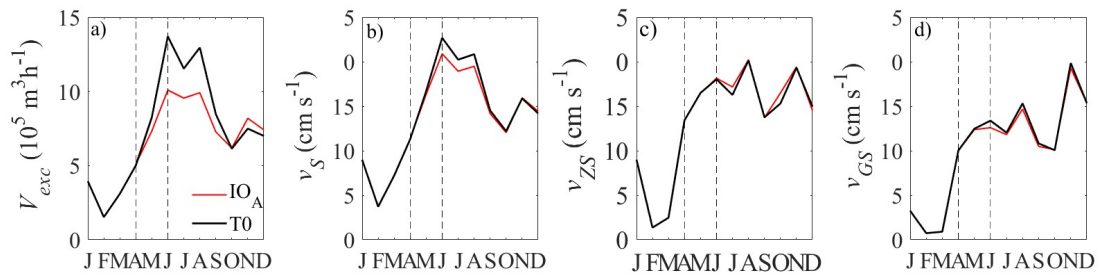


Figure S13. Results of the sensitivity analysis for the year 2010 at the sill and at the stations M_{GS} and M_{ZS} . The reference scenario was T0 (black line). The scenario with constant water level starting in April was called IO_A. The response of the system to the scenarios was analyzed at the sill comparing the monthly-mean water exchange (V_{exc}) and mean current speed (v_s) with the reference scenario, and at the stations M_{GS} and M_{ZS} comparing the monthly- and vertically-averaged current speed (v_{GS} and v_{ZS}) of IO_A with T0.

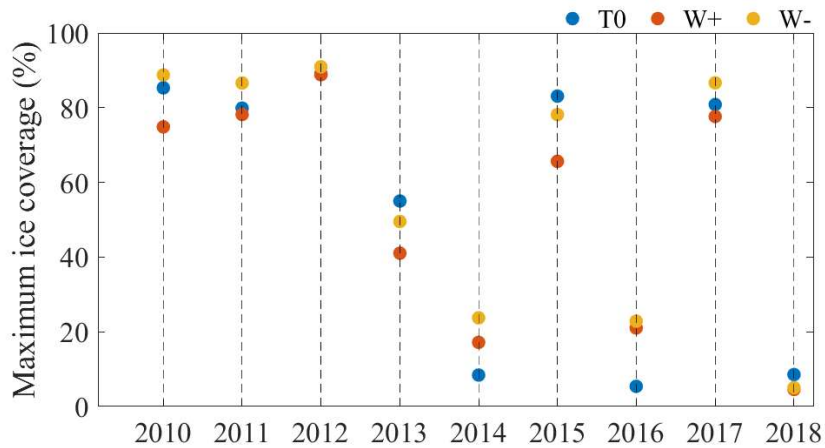


Figure S14. Maximum ice coverage of the lake surface during each winter in the scenarios T0, W+ and W- between 2010 and 2018.

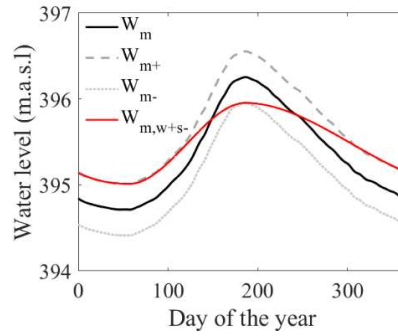


Figure S15. Seasonal water level scenarios. W_m represents the mean seasonal course of water level over the last 200 years which was measured in LLC, whereas $W_{m,w+s-}$ represents a 30 cm higher water level during the winter months and a 0.3 m lower water level during summer. The water level scenario W_{m+} considers a constant increase of 0.3 m with respect to W_m over the year, while W_{m-} a decrease of 0.3 m.

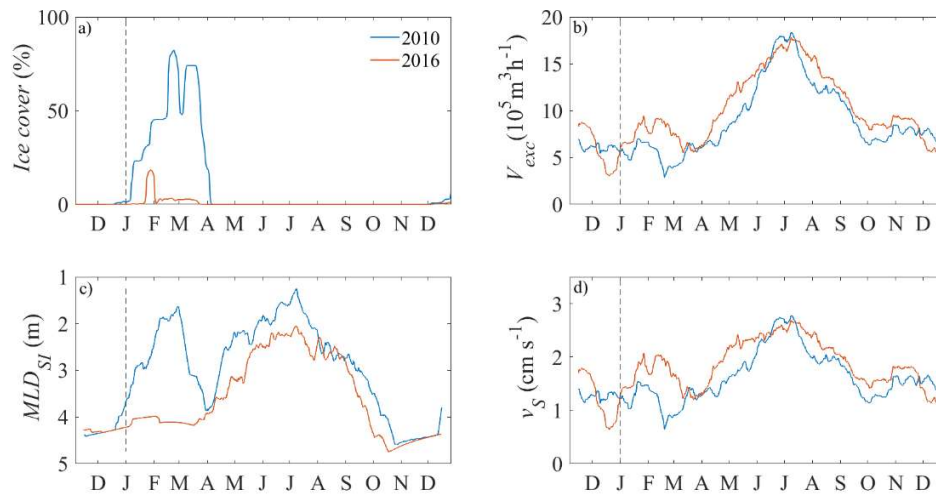


Figure S16. Seasonal course of water exchange V_{exc} , exchange velocity v_s and additional parameters for the scenario W_m . Seasonal pattern of a) percentage of lake surface covered by ice cover, b) water exchange V_{exc} , c) mixed layer depth at M_{Sl} , MLD_S , and d) exchange velocity across the sill v_s . Simulation results are provided for the year 2010 (blue), which was characterized by abundant ice cover, and for the year 2016 (red) which was characterized by little ice cover.

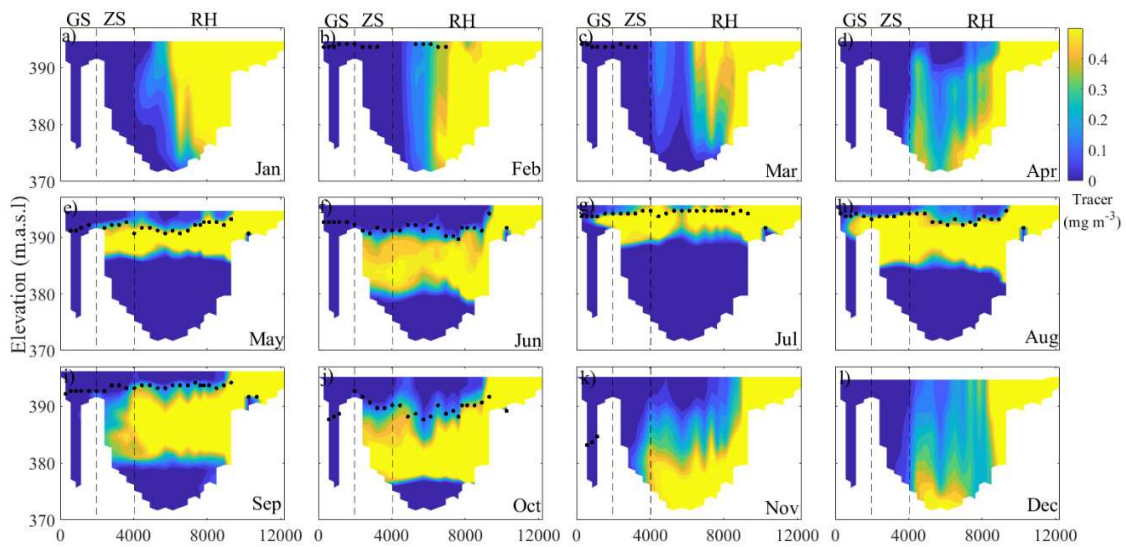


Figure S17. Spreading of the tracer along $\text{Trans}_{\text{I-G}}$ for the reference scenario in 2010. Panel a) to l) show the distribution of the tracer concentration 2 days after the beginning of the tracer experiments, which was re-started at the 1st day of each month. The black dots indicate the $\text{MLH}_{\text{I-G}}$. The dashed lines delimit the three sub-basins.

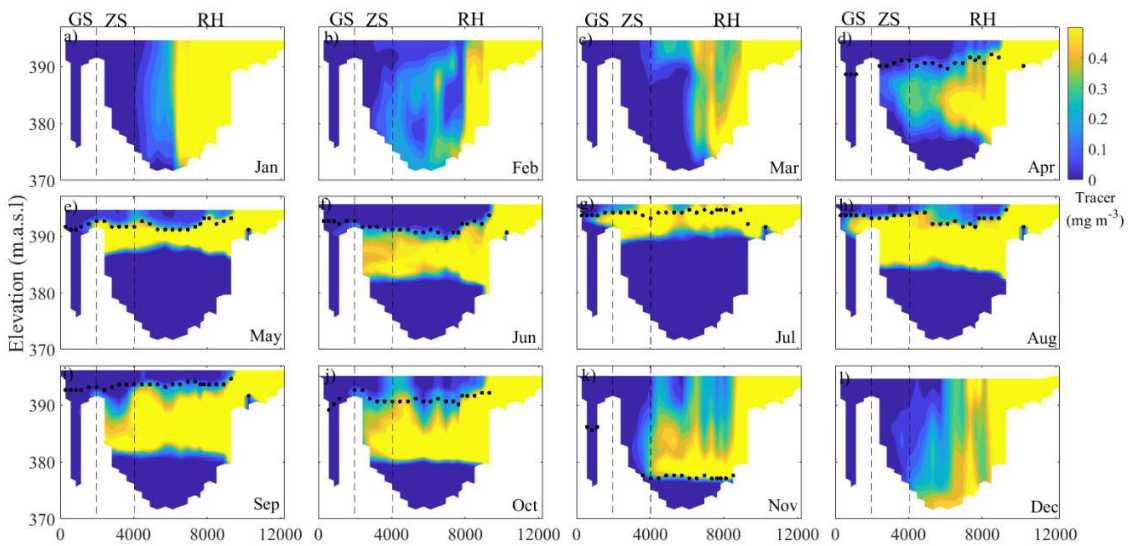


Figure S18. Spreading of the tracer along $\text{Trans}_{\text{I-G}}$ for the scenario T4 in 2010. Panel a) to l) show the distribution of the tracer concentration 2 days after the beginning of the tracer experiments,

which was re-started at the 1st day of each month. The black dots indicate the MLH_{I-G} . The dashed lines delimit the three sub-basins.

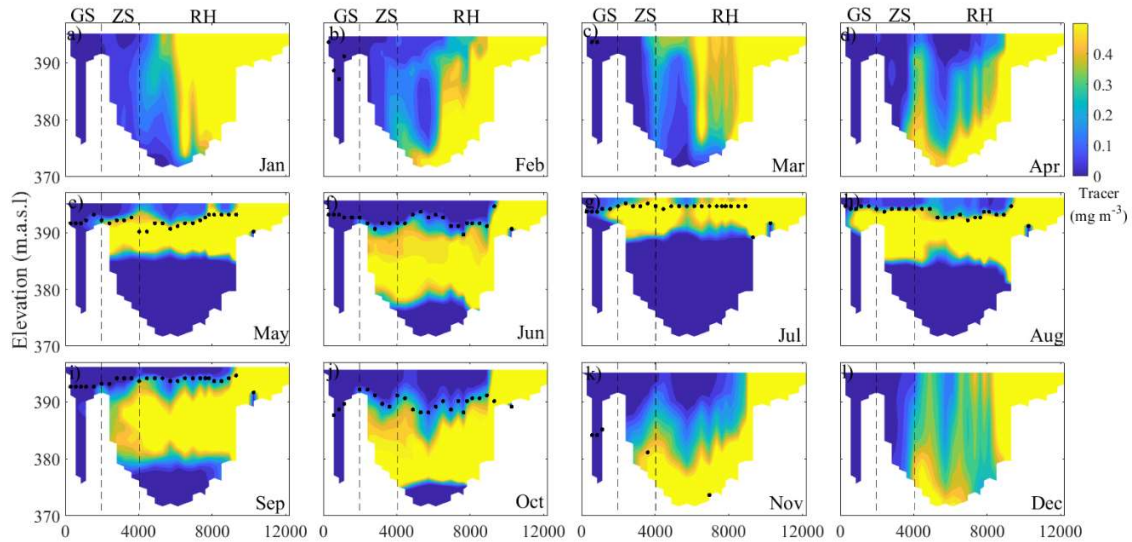


Figure S19. Spreading of the tracer along $Trans_{I-G}$ for the scenario W+ in 2010. Panel a) to l) show the distribution of the tracer concentration 2 days after the beginning of the tracer experiments, which was re-started at the 1st day of each month. The black dots indicate the MLH_{I-G} . The dashed lines delimit the three sub-basins.

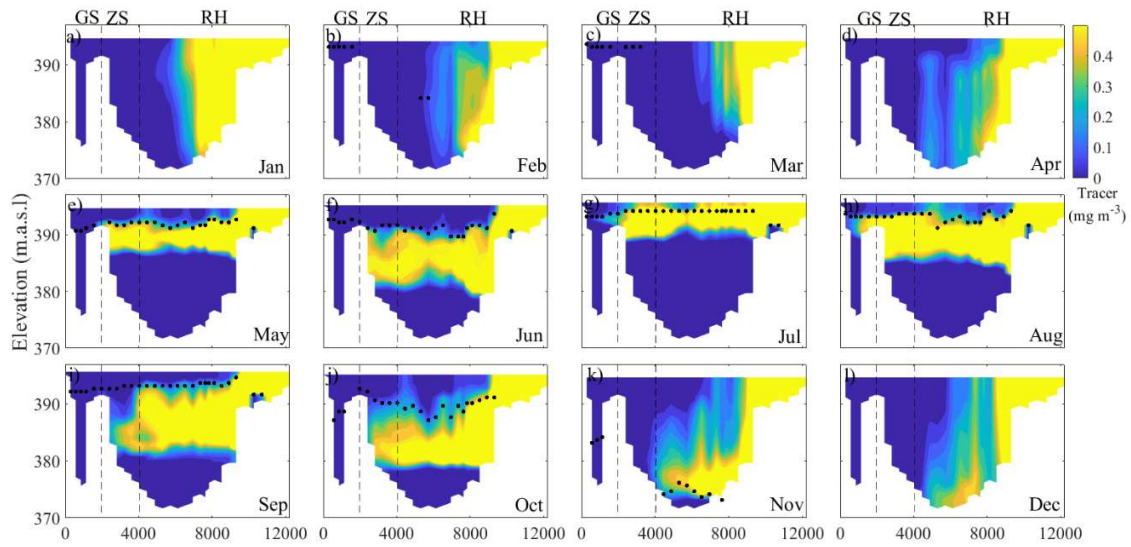


Figure S20. Spreading of the tracer along Trans_{I-G} for the scenario W- in 2010. Panel a) to l) show the distribution of the tracer concentration 2 days after the beginning of the tracer experiments, which was re-started at the 1st day of each month. The black dots indicate the MLH_{I-G} . The dashed lines delimit the three sub-basins.

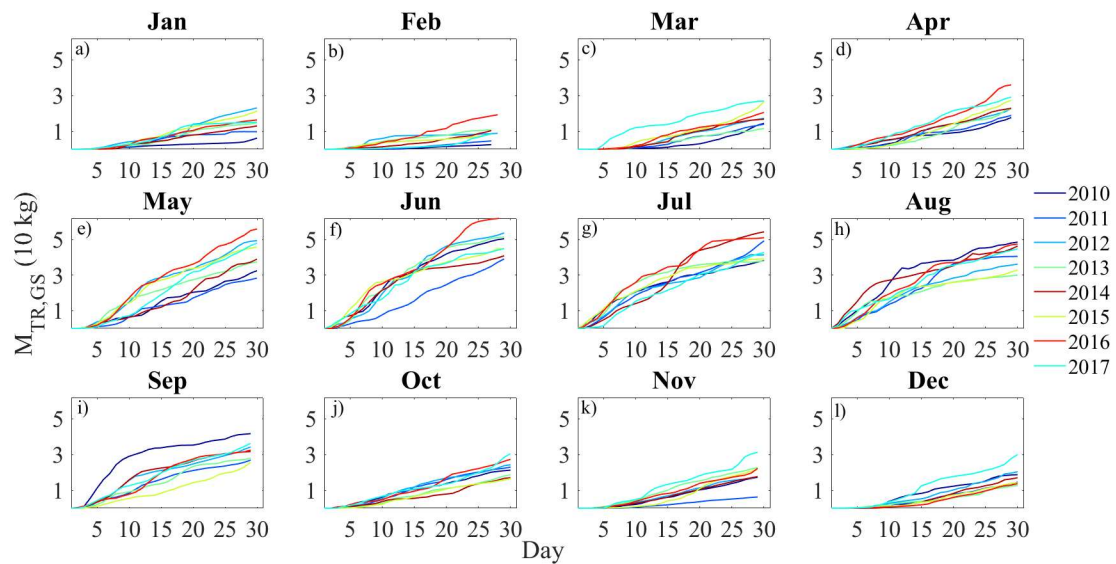


Figure S21. Time series of the tracer mass in GS ($M_{TR,GS}$) for each month and for all years.

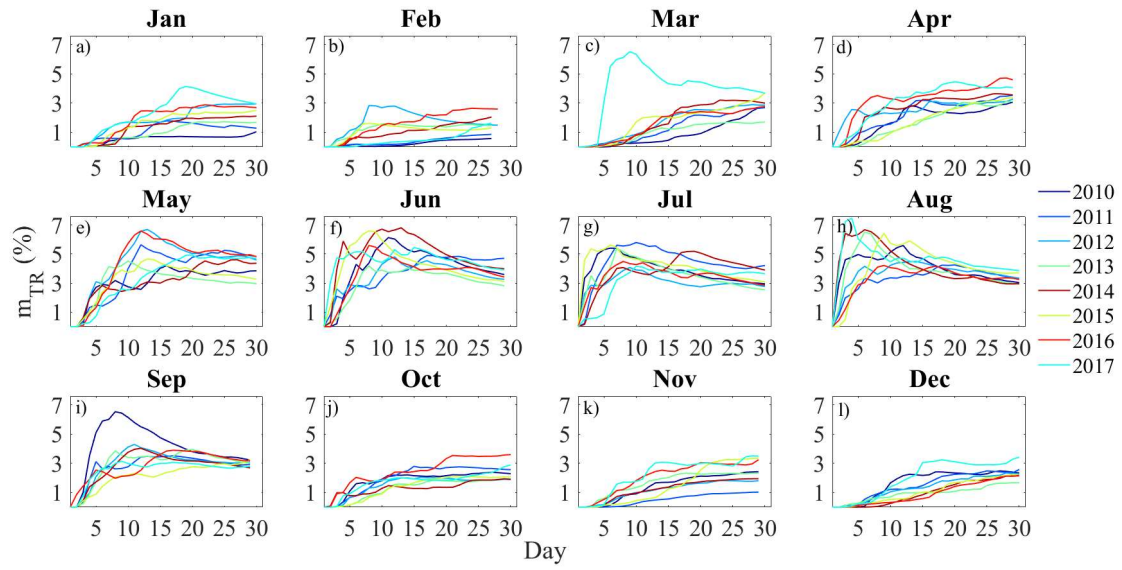


Figure S22. Time series of the fraction of the tracer mass in GS ($M_{TR,GS}$) divided by the mass of tracer introduced in the lake (M_{TR}), i.e. m_{TR} for each month and for all years.